DELFT UNIVERSITY OF TECHNOLOGY

FACULTY OF AEROSPACE ENGINEERING

SUSTAINABLE ENERGY TECHNOLOGY

MASTER THESIS

Hydrogen turbines

Effects of an increasing power density
on the levelised cost of hydrogen

F.D. de Klerk
4961137

supervised by:
Dr.ir. M.B. Zaayer
and
Ir. J.H.G.H. Groenemans

DEPARTMENT OF WIND ENERGY

January 31, 2021

Summary

In the current world, fossil fuels and non-renewable energy sources are being phased out and renewable energies are taking their place. Electrical energy from these renewable energies are more difficult to store than fossil fuels. Transportation and feedstock for industries can also not always be supplied through electricity. Here, hydrogen has the potential to be a good alternative, clean energy source. However, hydrogen is currently either not produced in a renewable manner (grey hydrogen), or renewable but too expensive (green hydrogen). Grey hydrogen is less expensive at a cost of around 1.50 €/kg, while green hydrogen has a cost of 2.50 - 5.00 €/kg. A new method to produce green hydrogen at a lower cost is the hydrogen turbine developed by HYGRO [1]. This method uses an integrated electrolyser system in an existing wind turbine to produce green hydrogen and has the potential to drop the cost of green hydrogen to a more competitive level.

Since this new method changes design questions of the wind turbine, a potential increase in specific power, along with a decrease in cost of hydrogen (expressed in levelised cost of hydrogen, or LCoH) is expected. In order to research these effects, this thesis investigated the effects of an increased specific power on the cost of the components of the turbine and its design, as well as the amount of hydrogen it was able to produce. This investigation was done through a model along with a case study to determine the results for a specific case. The increase in specific power was achieved by increasing the power rating of the turbine, but maintaining a constant rotor radius and maximal rotor speed. The case study performed investigates the effects based on a 15 MW reference turbine, which has a specific power of 331 W/m^2. Its power rating was increased from 15 MW up to 35 MW and the resulting costs and production amount were compared to determine an optimal point were the resulting LCoH would be lowest.

The result of the case study suggests that if the 15 MW reference turbine was converted to a hydrogen turbine, the optimal power rating would be in the range of 25-30 MW, where an LCoH of around 1.69 €/kg was achieved. These power ratings are equal to a specific power range of 553 - 663 W/m^2 or 66 - 100 % higher than the reference. Through an error analysis, the results were validated and determined to have a reasonable degree of certainty. The main component of the model that could be improved upon to increase its robustness is the wake loss model, which was not precisely modelled but does have a significant effect on the results.

The increase in specific power suggests that hydrogen turbines have the potential to perform at higher power ratings than the wind turbine it is based on. This would allow the green hydrogen cost to drop significantly, down to a value were it is nearly competitive with grey hydrogen.

Nomenclature

Abbreviations

AC	Alternating current
AHP	Annual hydrogen production
BoP	Balance of Plant
CCUS	Carbon capture, use and storage
DC	Direct current
EDI	Electrodeionization
EUR	Euro
GBP	British Pound Sterling
IEA	International Energy Agency
LCoE	Levelised cost of electricity
LCoH	Levelised cost of hydrogen
MD	Membrane distillation
NPV	Net present value
NREL	National Renewable Energy Laboratory
PEM	Polymer electrolyte membrane
THP	Total hydrogen production
USD	U.S. Dollar
WF	Wake factor
WL	Wake losses

Greek symbols

γ	Efficiency loss
ρ	Volumetric mass density
λ	Tip speed ratio
σ	Stress
χ	Monopile depth factor
Θ	Ratio between wall thickness and outer diameter
Ξ	Cost scaling factor of generator
Ω	Generator speed

Other symbols

A	Area
A	Swept area of turbine
a	Scale parameter

C	Constant
C	Cost
C_F	Blum constant for no moment
C_M	Blum constant for no force
C_P	Power coefficient
C_Q	Torque coefficient
C_T	Thrust coefficient
D	Diameter
d	Discount rate
F	Force
f_b	Factor between reference and new thickness as a result of bending stress
f_c	Factor between reference and new thickness as a result of compression stress
F_g	Gravity force
F_n	Normal force
F_t	Tangential force
f_u	Uncertainty factor
g	Gravitational acceleration
h	Depth
h	Tower height
H_2	Hydrogen
I	Area moment of inertia
i	Inflation rate
k	Shape parameter
L	Distance
M	Moment
m	Mass
P	Power
p	Perpendicular distance
Q	Torque
R	Rotor radius
r	Interest rate
s	Dimensionless distance
T	Lifetime
T	Thrust

t	Thickness
t	Time
t_f	Thickness factor
t_w	Wall thickness
U	Wind speed
V	Volume
X	Blade mass correction factor
y	Distance to neutral axis
z	Height coordinate
z'	Height level

List of Tables

List of Figures

Contents

1 Introduction

1.1 Motivation

In the current world, fossil fuels and non-renewable energy sources are being phased out and renewable energies are taking their place. Electrical energy has popular alternative sources such as wind and solar power, but these sources are more difficult to store. Furthermore, energy needed for transportation and feedstock for industries can not always be supplied through electricity. Here, hydrogen (H_2) can be a good alternative energy source. However, hydrogen is currently either not produced in a renewable manner, or is too expensive. In order to fulfil this role, it is expected that hydrogen will be a driving force in the energy transition. As can be seen in figure 1, the renewable hydrogen production is expected to increase seventeen-fold between 2020 and 2030 [2].

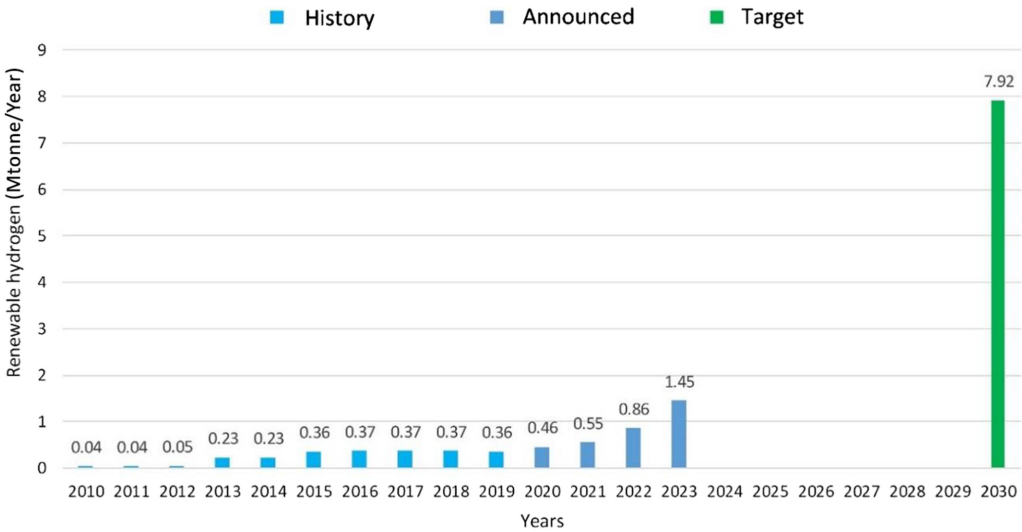

Figure 1: Low-carbon hydrogen production, 2010-2030, historical, announced and in the Sustainable Development Scenario, 2030 of IEA [2]

A clear distinction needs to be made between "grey", "blue" and "green" hydrogen production. Grey hydrogen is produced using carbon intensive processes such as steam methane reforming. The carbon emitted during production is not compensated and released into the atmosphere. Blue hydrogen uses carbon capture, use and storage (CCUS) to minimise carbon emissions. Green hydrogen is the only sustainable variant of the three, where all hydrogen is produced using renewable energy sources such as wind or solar.

The current cost competitive hydrogen production is carbon intensive, or grey. The costs associated with both grey and blue production methods are shown in figure 2. As can be seen, grey hydrogen cost ranges from 1 - 1.75 $/kg or 0.85 - 1.50 €/kg, while blue hydrogen ranges from around 1.45 - 2.40 $/kg or 1.25 - 2 €/kg. In order for the hydrogen produced by renewable energy sources to be cost competitive, its price will have to be lower than or equal to that of grey hydrogen. This sets a clear goal for the optimal cost of hydrogen to be lower than 1.50 €/kg to be competitive in Europe. Current green hydrogen prices range from 2.50 - 5.50 €/kg [3], clearly showing the large price gap.

One possible method of green hydrogen production is the use of offshore wind farms. Here, the energy produced by the wind farm is converted to hydrogen using electrolysers. The normal design would would have the energy produced transported to shore, where it is then converted to hydrogen in the aforementioned electrolysers. Another design is to use a centralising substation at sea with electrolysers, followed by hydrogen transport through pipelines. In 2021, the first pilot for such a system will start off the coast of The Hague in the PosHYdon project [5]. The first system is plagued by high transport to shore costs, stemming from the cost of the cables used to transport the electricity. This makes it an illogical option to expand on. The second option improves the idea, but conversion losses are still present and the cost of the necessary sub-station also drive up the price. A third variant of this idea of offshore wind combined with

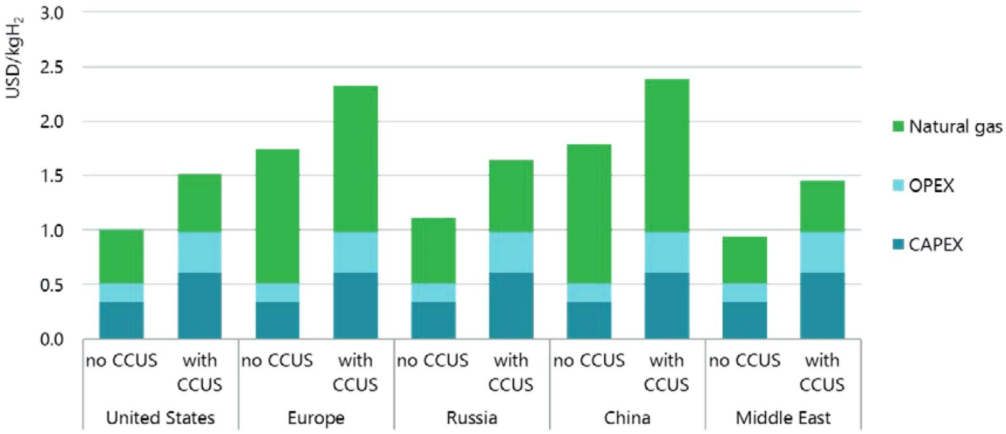

Figure 2: Hydrogen production cost using natural gas in selected regions 2018 [4]

electrolysers has been designed by the company HYGRO [1]. Here, the electrolyser is integrated into the turbine itself, removing the need for a sub-station as well as several other components, such as a DC-AC inverter and a transformer, which will lower the final cost of the turbine. These turbines are also known as hydrogen turbines. Another advantage of hydrogen turbines is the big decrease in conversion losses due to fewer conversion steps being necessary. For hydrogen production in these hydrogen turbines to be a viable alternative, it will need to have a price after transportation to shore close to current, grey hydrogen production methods.

1.2 Problem definition

The hydrogen turbine by HYGRO is a turbine that has an integrated electrolyser, does not need an external power connection and outputs hydrogen into a pipeline at 100 bar. The integration of the electrolyser lowers electrical conversion losses and transport losses. Furthermore, several components of a wind turbine become irrelevant and are removed, lowering the cost of the turbine. Therefore the LCoH of HYGRO's hydrogen turbine is "many times lower than the production of hydrogen in a separate electrolysis process connected to the electrical infrastructure." [6]. Furthermore, the hydrogen turbine allows for new possible optimal designs of the turbine. A normal wind turbine is optimised with respect to levelised cost of electricity (LCoE), while the hydrogen turbines can be optimised for the levelised cost of hydrogen (LCoH). Lastly, the production of hydrogen is less affected by the intermittent nature of wind energy. Normal wind turbines are currently being designed to supply a more constant base load and minimise the effects of the intermittent nature of wind energy. To achieve this, turbines are designed with a lower specific power, since this allows the turbine to operate at rated power more often. The trend in specific power of the installed turbines can be seen in figure 3. Here, the average specific power of a turbine clearly has a downward slope between the years 1998 and 2014. A hydrogen turbine is not constrained by the need for a constant power production, since the power is converted to hydrogen. It is designed to optimise for a maximum energy conversion. Therefore, hydrogen turbines can be designed for higher specific power than a normal wind turbine.

HYGRO expects that due to the optimisation with respect to the LCoH instead of LCoE, current normal wind turbines could be redesigned to higher specific power hydrogen turbines. Their reasoning for a new design stems from the fact that several components of a normal wind turbine are no longer present or are replaced, changing the cost of the turbine. The thought that this would also result in a new optimal specific power is based on the expectation that the increasing costs are more than compensated by the increasing production levels at higher power densities. The increase of production at a higher specific power does not continue on endless, due to the amount of wind energy available. At some point, taking more energy from the wind will no longer be feasible or profitable.

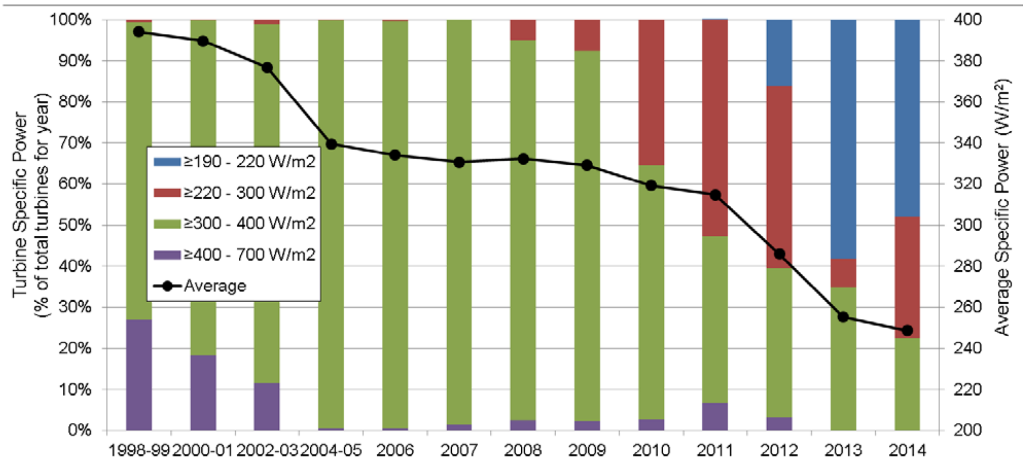

Figure 3: Trends in turbine specific power in the USA [7]

1.3 Research objectives and approach

This thesis encompasses one main goal concerning the previously described hydrogen turbines. This is:

- Provide advice on a more optimal specific power of hydrogen turbines, based on the calculated LCoH associated with a range of specific powers

The increase of specific power of the hydrogen turbine is investigated through a model, which is used to determine the cost and production at those specific powers, on which the LCoH is based. In this model, the increase is achieved by maintaining a constant rotor radius, combined with an increase of the power capacity of the turbine. This increase in specific power will result in changes of the four design drivers of the turbine. These design drivers are the power capacity, the torque, the thrust and the gravity force. How these drivers scale with an increasing specific power is described. The scaling of these drivers will also affect the cost and mass of the components of the turbine. Furthermore, the increase in specific power not only affects the cost of the turbine, but also the amount of hydrogen it is able to produce. The scaling of the production is discussed as well. Both the cost and production are combined in the LCoH

In order to gain insight in the exact effects of a higher specific power, a case study is performed. Here, the model is run for a 67 wind turbine wind farm in the North Sea. The turbine scaling is performed with as a starting point the IEA 15 MW reference turbine [8]. The case study investigates the effects of an increasing specific power from 331 W/m^2 up to 774 W/m^2. For a multitude of points between these two extremes, the LCoH is calculated. The lowest LCoH would suggest a more optimal design of the hydrogen turbine at that specific power.

1.4 Thesis structure

This thesis starts of with an explanation of the system specifications for the case study. Included is an explanation of what a hydrogen turbine is, what components from a normal wind turbine are left out and a break down of the extra components of a hydrogen turbine compared to a normal turbine. Lastly, modelling assumptions are described.

Following the first chapter, the chapter modelling discusses the inner workings of the model. Here, the way of calculating the LCoH is given. Furthermore, the effects of a change in specific power on the design drivers is described, as well as the scaling of the components of the hydrogen turbine. Finally, the method of determining production levels is elaborated on.

The fourth chapter contains the case study description as well as the boundary conditions that apply to it. The results of the case study are also given and discussed, along with a description of the optimal hydrogen turbine. Furthermore, in order to validate the result, an error analysis is performed through investigating the effects of variable inputs into the model.

The last chapter draws conclusions from the results in chapter 4. The work done is also discussed. This entails a description of the current shortcomings within the research, as well as possible areas of further research and recommendations on improvements.

An appendix is also present. The information that was too extensive for the main report is placed here.

2 System configuration

Within this section, the workings of a hydrogen turbine system are described. Information is given as to what components such a turbine contains and what the components are. Furthermore, modelling assumptions made during this thesis are elaborated on.

2.1 What is a hydrogen turbine

Firstly, a short description of the workings of a hydrogen turbine is fitting. A hydrogen turbine is a wind turbine that, within the turbine itself, converts wind energy to hydrogen, which is transported to land through pipelines.

The company HYGRO has made some changes and advances in the design of such turbines. This turbine uses most of the components of an original wind turbine, but removes some and adds some others. In order to create a clear and concise overview of what a hydrogen turbine is, a description is provided below. It should be noted that this thesis only looks at offshore turbines. Some details might differ onshore.

There are two major adaptions from a normal wind turbine to a hydrogen turbine, other than the addition of electrolyser systems. These two are the lack of requirement for an external power connection and the removal of several electricity conversion steps within the turbine since the electrolysers run on DC power.

Since the system no longer requires an external power source and the product produced is transported through pipelines instead of cables, the entire outer cabling system is removed. Furthermore, since the hydrogen is produced at the turbine itself and pumped into a pipeline system, there is no longer a need for sub-stations either. The pipelines running from the different turbines can be combined below water into a bigger pipeline system that transports the hydrogen to land. The removal of both the cables and the sub-station are two big cost decreases for wind farms with hydrogen turbines.

The removal of electricity conversion steps mainly stems from the need of electrolysers for direct current (DC) electricity. Figure 4 depicts the conversion steps in a normal turbine. First the electricity produced by the generator is converted from alternating current (AC) to DC, followed by a DC/AC converter. The AC power is then filtered and guided through a transformer. Onshore, it is fed into the grid from that point. In offshore turbines, the cables transport the power to a substation, where the voltage is increased and, depending on how far offshore, the power is once again converted from AC to DC.

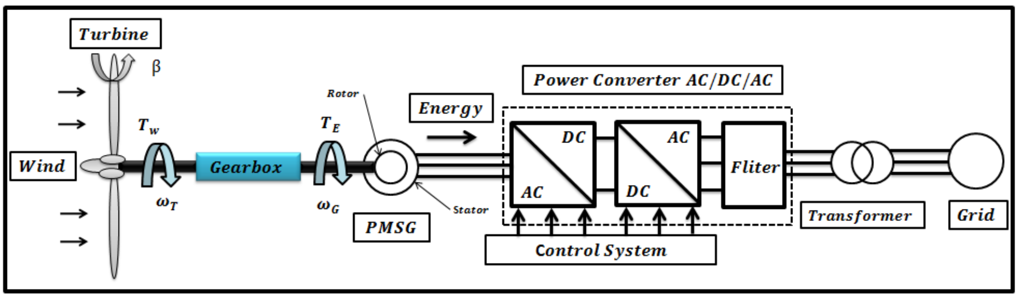

Figure 4: Overview of the internal system of a normal wind turbine [9]

Due to the lack of need for AC as an output, the conversion steps after the first AC/DC converter are removed. Within a hydrogen turbine, the electricity produced at the generator is only converted from AC to DC which is immediately plugged into the electrolysers without further conversion steps, removing another major cost item.

The main additions in a hydrogen turbine are electrolyser stacks, a water purification system, compressors for the hydrogen, a battery and a fuel cell. Lastly, pipelines are also added in order to transport the hydrogen to land. All other components of a wind turbine that have not been mentioned above are the same in both a normal and a hydrogen turbine.

A simplified overview of the internal system of a hydrogen turbine, where some details are omitted for clarity sake, is given in figure 5. Firstly, the black line of electricity is produced in the direct-drive generator from the rotor rotation due to wind energy. This generator electricity is AC, which will have to be converted to DC. This DC power is used in several places. Firstly, it is used to pre-charge the electrolysers of the hydrogen turbine system in order to produce the orange line hydrogen. Furthermore, it is connected to the two water purification steps, the compressor, the battery, the fuel cell and the turbine and electrolyser control system. The battery can be charged using electricity from the generator. Both the fuel cell and battery are available in case of either a failure or at start-up, when electricity is needed but not (yet) being provided by the generator. The blue lines depict the water flows within the system, starting at the membrane distillation and going through the electrodeionization module to supply the purified water to the electrolysers. The electrolysers produce hydrogen at 30 bars and oxygen, which is vented out. The hydrogen is further compressed by the compressor system up to 100 bars, after which it is delivered to the pipeline depicted as the yellow line, ready to be transported to shore. The entire system of electrolysers, water purification, fuel cell, battery and compressors is placed within the transition piece of the tower. Even with an increasing power rating, this will fit, since two 2.5 MW of electrolyser stacks used by HYGRO fit in a 1 m^3 volume.

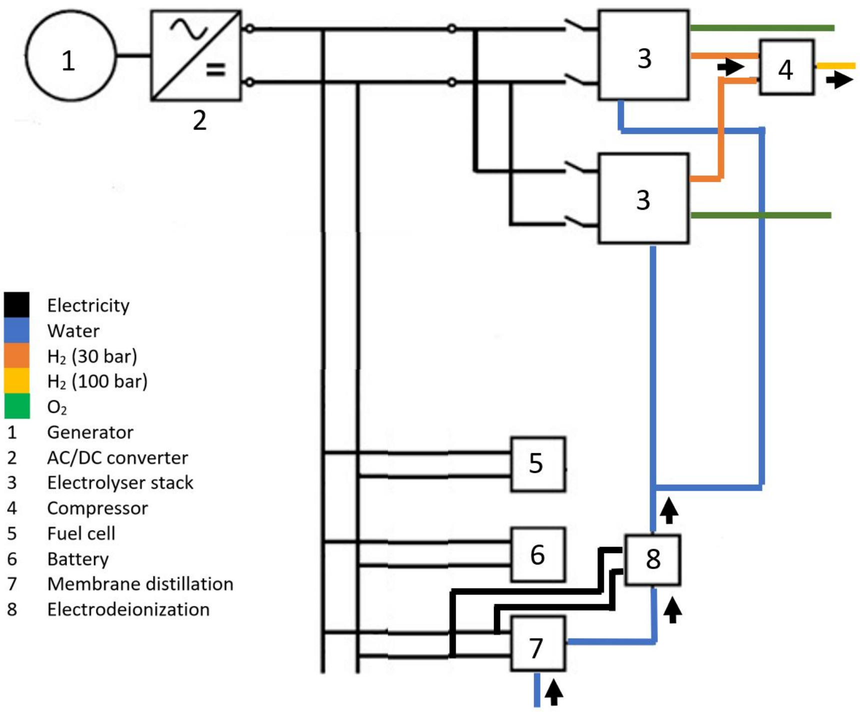

Figure 5: Overview of the internal system of a hydrogen turbine, adapted from the patent request of HYGRO

2.2 Components of the hydrogen turbine

2.2.1 Electrolyser

The electrolysers used in the hydrogen turbines designed by HYGRO are PEM electrolyser and supplied by PlugPower [10]. All sizes and other values are based on what PlugPower has shared with HYGRO as to what they can produce, including measurements of their product.

PEM electrolyser were chosen instead of alkaline electrolysers due to the smaller size of PEM. As stated above, two 2.5 MW PEM electrolyser stacks fit in 1 m^3, while alkaline electrolysers are around three times bigger and won't fit into the allocated location of the transition piece [11].

The hydrogen produced by the electrolyser will be at most 30 bars, which will have to be further compressed to 100 bars for the pipelines by a compressor. The electrolysers are allowed to produce up to a temperature of 75 °C in order to increase their production levels. The maximum stack size is 2.5 MW. Therefore, several stacks are combined to achieve the necessary power rating. The electrolyser stacks have a current density of 2.3 A/cm^2.

The efficiency of electrolysers is highest at low input power, as later will be shown in figure 12. In order to maximise the use of this effect, HYGRO has developed a system where the initial aim is to spread the power over more electrolysers. This is done by having the number of stacks in operation be determined by dividing the available electric power by 500 kW. This enables a high efficiency and a longer life of the electrolysis system, since it's not operating at maximum power.

2.2.2 Compressor

Since the hydrogen at the electrolyser output is at 30 bars and the required pressure for the pipeline is 100 bars, a compressor system is needed. HYGRO uses a piston compressor system by Howden Compressors [12]. This compressor will be a piston compressor that is already applied in the current industry. It also has special seals that allow it to compress up to an operational pressure of 200 bars at most.

2.2.3 Fuel cell and battery

In order for the hydrogen turbine to be able to function without an external power connection, both a fuel cell and a battery are available. During normal operations, the generator is able to produce the necessary electricity for the control systems and water purification. However, at times of no wind or at start up, some other source of electricity is necessary for the functioning of the turbine. A small battery is the first back-up power source that has immediate energy available and therefore provides time for the fuel cell to start up. The fuel cell can be used to convert some of the previously produced hydrogen into electricity for steady operation and start-up.

2.2.4 Water purification

Offshore wind turbines have an abundance of sea water around them that can be used for electrolysis. However the water needed for a PEM electrolyser needs an extremely high purity. In order to achieve this, two water purification steps are used. Firstly, membrane distillation (MD) desalination technology is used, followed by electrodeionization (EDI).

MD is a desalination process that uses heat to achieve a phase change in the water. It is "especially well suited for high salinity feed water" [13] such as sea-water. MD uses heat to evaporate water at a hydrophobic membrane that only allows water vapour to pass through, not the liquid water that still contains salt [14].

EDI is used next as a polishing treatment to remove most of the last ions from the water. EDI is a process that makes use of "electrochemical water deionization using ion-specific membranes, mixed-bed resins and a direct current voltage" [15]. By using EDI, the specific conductivity can be lowered to less than $0.056\ \mu S/cm$ [16], which is pure enough for the electrolyser system in a hydrogen turbine.

2.2.5 Pipelines

In order to transport the 100 bar hydrogen safely to shore, pipelines are used. These pipeline are High Pressure Flexible Composite Pipe Systems by SoluForce [17]. This specific product is designed for hydrogen transportation, making it a good solution for transportation. The main advantage of a composite pipe system designed for hydrogen is that it is flexible. Therefore, it is easier to install and thus lowers installation cost to a level similar to that of laying a cable. Permeation through the material is low, resulting in less lost product. Furthermore, since it does not contain steel, a composite pipe does not suffer from hydrogen embrittlement and corrosion. [18].

2.3 Model boundary conditions

The model created during this thesis aims to find the LCoH of several different power capacities for a similar hydrogen turbine. In normal situations where a higher power rating of wind turbine is required, the rotor diameter is increased. However, within this thesis, the rotor diameter is kept constant as a constraint. Furthermore, the maximum rotational speed is also kept constant at the reference turbine's speed. Typically, the tip speed of offshore wind turbines is restricted to around 100 m/s [19], which is the tip speed most offshore turbines are designed for. Since the maximum rotational speed and rotor diameter are kept constant, an increasing power capacity leads to an increase of the rated wind speed, which itself also results in a lower tip speed ratio and power coefficient. By increasing the tip speed too much, the blades will start acting as a solid disk, decreasing the amount of energy it can convert from the wind. Lastly, the hub height is kept constant throughout this project as well.

The scope entails the results of an entire wind farm, not just a single turbine. This was done, because by excluding relevant areas for a wind farm such as pipelines and operations costs and decreasing the amount of product produced, the result will be incomplete and incorrect. Since the costs necessary for an entire wind farm include more fixed values, the location of the optimal power rating changes and becomes more reliable compared to a scope that excludes these fixed costs.

The base size of the wind farm is set around one GW. This size was chosen due to the information available for a one GW offshore wind farms in a report by BVG Associates for the British Crown Estate [20]. This report assumes one hundred 10 MW turbines and therefore gives a reasonable baseline for the cost of multi-megawatt hydrogen turbines.

3 Modelling

Within this chapter, the entire thought process and methods behind the modelling and calculations are described. To start off, a description of the LCoH is given. This is followed by an explanation as to how the relevant design drivers scale in the context of this thesis. Next, all components of a wind farm with hydrogen turbines are discussed. Lastly, an explanation on the determination of the production levels is given. The goal is to create a model that determines the cost and production levels for hydrogen turbines with different power capacities and from there allows insight in a more optimal power capacity. The entire model can be seen in appendix A.

3.1 Levelised cost of hydrogen

In order to compare the production levels at each power rating with their associated cost, the levelised cost of hydrogen (LCoH) is introduced. This LCoH is cost price for each kilogram of hydrogen produced and brought to shore. The LCoH is calculated according to equation 1:

$$\text{LCoH} = \frac{\sum_{t=1}^{T} C_t \cdot (1+d)^{-t}}{\sum_{t=1}^{T} AHP_t \cdot (1+d)^{-t}} \tag{1}$$

Where t is the relevant year, T is the lifetime, C_t is the cost for relevant year t, AHP_t is the annual hydrogen production in year t and d is the discount rate.

Since some costs are incurred later on in the project, to create a proper comparison, these costs will have to be discounted to present day values. The same is done for future production. Examples of future costs are yearly maintenance and operations costs or the decommissioning at the end of the design life. All of these costs are assumed to be paid at the end of each relevant year. A method to calculate the present day value of these costs is using the net present value equation (as seen in equation 2).

$$\text{NPV} = \sum_{t=1}^{\text{lifetime}} \frac{C_t}{(1+d)^t} \tag{2}$$

Here, t is the year, C_t is the cost in the relevant year and d is the discount rate. This discount rate is calculated using equation 3:

$$d = \frac{1+r}{1+i} - 1 \tag{3}$$

Where r is the expected interest rate and i is the expected yearly inflation.

The NPV is generally used to evaluate the profitability of an investment over the lifetime of the chosen project. This method can however just as well be used to calculate the amount of money that is needed in the present in order to pay off costs in the future, assuming that it would yield the chosen interest rate up to the chosen point in time in the future. The production is discounted using the same discount rate as the cost. The production is discounted, since future production is less valuable than current production.

The LCoH is calculated for each relevant power rating in this model, which allows for easy comparison between the results. A lower LCoH is better, since it results from lower costs to produce hydrogen, therefore, at the point were the LCoH is lowest, the optimal power rating is found.

As stated in the introduction (section 1.1), for the green hydrogen to be competitive with grey hydrogen, the LCoH needs to be lower than at least 1.50 €/kg.

Within this thesis, different currencies are used. In order to normalise these, 2020 euros are the currency in which all used data is expressed. Monetary amounts in USD from the past are converted to 2020 values using an online inflation calculator [21]. Here, the amount is corrected using the inflation over the relevant period. The exchange rates used are 1.15 GBP/EUR and 0.85 USD/EUR, where both are set around the average exchange rate in 2019 [22].

3.2 Overview of scaling methods

The overarching goal of this thesis is to determine the effects of an increased power density on the LCoH. In order to achieve this, the amount the cost of the hydrogen turbine increases with higher power capacities must be known. The increased cost will scale differently for different components of the turbine and the entire wind farm. In order to create an overview, table 1 below states all the components taken into account in this model and gives their design drivers. Furthermore, the scalable parameters that drive the design of each component are described below. It should be noted that this model only looks at static conditions and has not taken into account dynamic effects at higher power capacities or different turbine designs. Therefore, the design will be a result of the extremest static conditions for each power capacity, which occur at rated wind speed. As stated in section 2.3, the scaling is constrained by a constant rotor diameter, hub height and maximum generator speed. Lastly, the modelling sometimes requires the availability of a reference turbine in order to determine the scaling for some components. When this is required, the necessary value is denoted with subscript ref.

Table 1: Overview of components and their design drivers for scaling

Component	**Power**	**Thrust**	**Torque**	**Gravity force**
Electrolyser system	X			
Compressor	X			
Converter system	X			
Generator	X		X	
Pipeline	X			
Blades		X	X	
Hub				X
Bedplate				X
Tower		X		X
Transition piece		X		
Monopile		X		
Installation turbine				
Installation pipeline				
Decommissioning wind farm				
Operations				
Maintenance				
Battery				
Fuel cell				
Yaw system				
Pitch system				
Bearings				
Shaft				
Miscellaneous components				
Controller system				

3.2.1 Design driver: Power

Since the scaling is based on an increasing power capacity of the turbine, power is the main driver that all other drivers can be related back to. Furthermore, since the rotor diameter is kept constant, the change in power capacity is the same as the change in specific power. The change in power capacity will not only affect the design drivers, but also other wind turbine variables such as the rated wind speed.

3.2.2 Design driver: Thrust

The modelling of the change in thrust due to a change in power capacity uses an iterative process where several standard equations for wind turbines are used. These are equation 4, 5 and 6.

$$\lambda = \frac{\Omega R}{U_{rated}} \tag{4}$$

$$C_P = \frac{P}{\frac{1}{2}\rho A U_{rated}^3} = \frac{P}{C_1 \cdot U_{rated}^3} \tag{5}$$

$$C_T = \frac{T}{\frac{1}{2}\rho A U_{rated}^2} = \frac{T}{C_1 \cdot U_{rated}^2} \tag{6}$$

Where in order of appearance:

λ	= Tip speed ratio	$[-]$
Ω	= Generator speed	$[rad/s]$
R	= Rotor radius	$[m]$
U_{rated}	= Rated wind speed	$[m/s]$
C_P	= Power coefficient	$[-]$
P	= Power	$[W]$
ρ	= Density of air	$[kg/m^3]$
A	= Swept area of turbine	$[m^2]$
C_1	= Constant	$[-]$
C_T	= Thrust coefficient	$[-]$
T	= Thrust	$[N]$

Here, equation 4 describes the tip speed ratio, equation 5 the power coefficient and equation 6 the thrust coefficient. In both the equations for the power and thrust coefficient, the density of air and the swept area of the turbine are kept constant, since the hub height and rotor diameter don't change. Furthermore, the maximal generator speed is also kept constant as stated before.

The steps used to determine the trust are described below.

1. A new power rating P is used in equation 5 along with the original power coefficient C_P of a reference turbine. The area A and density ρ are constant throughout this process so can be rewritten together with the $\frac{1}{2}$ as constant C_1
2. This results in a rated wind speed U_{rated}, which can be used in equation 4 to determine a new tip speed ratio λ, since the Ω and R terms are constant
3. This λ is compared to the $C_P - \lambda$ curve of a turbine. An example of such a curve can be seen in figure 6
4. Since these new found C_P, λ and U_{rated} affect each others values, the previous three steps are repeated, where in step 1, the C_P is changed to the new found C_P. These steps are repeated until the difference between the new C_P, λ and U_{rated} differ less than 0.01% from their values after the first iteration
5. The final value of λ is used in a C_T - λ curve to determine the final thrust coefficient C_T. An example of such a curve can be seen in figure 7
6. Combining both the determined C_T and U_{rated}, equation 6 is used to calculate the final thrust value
7. When modelling for several power capacities, creating a proper fit through the thrust data points is advised

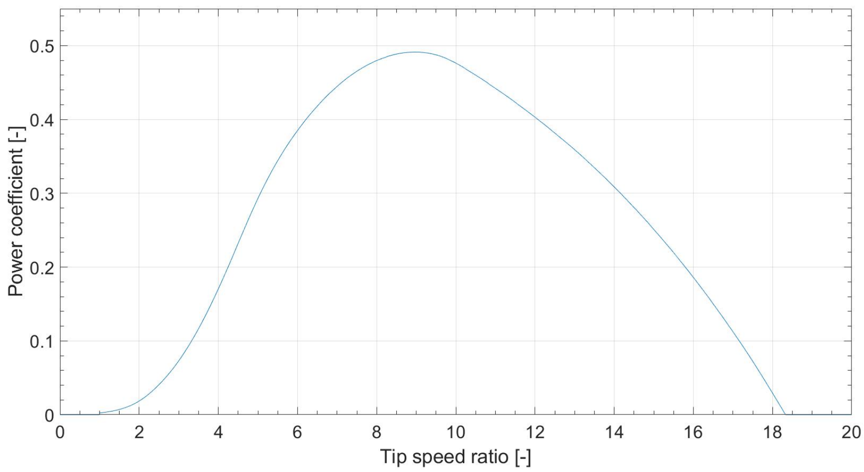

Figure 6: $C_P - \lambda$ curve for a 15 [MW] wind turbine

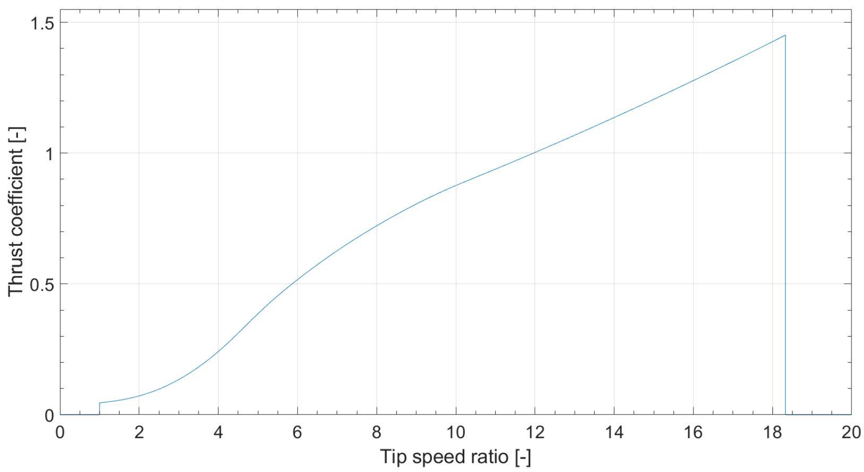

Figure 7: $C_T - \lambda$ curve for a 15 [MW] wind turbine

3.2.3 Design driver: Torque

The increase in torque is dependent on the increase in power capacity and generator speed, since:

$$C_Q = \frac{C_P}{\lambda} \tag{7}$$

where C_Q is the torque coefficient, C_P is the power coefficient and λ is the tip speed ratio. The power coefficient and tip speed ratio are given above in equation 4 and 5. The torque torque coefficient can be written as:

$$C_Q = \frac{Q}{\frac{1}{2}\pi R^3 \rho U_{rated}^2} \tag{8}$$

where P is the power capacity, ρ is the air density, A is the swept area by the turbine, U_{rated} is the rated wind speed, Q is the torque at rated wind speed, R is the rotor radius and Ω is the maximal generator speed. The rotor radius, air density, swept area and maximal generator speed are all kept constant, as stated before. By filling in equation 4, 5 and 8 into equation 7, the following equation is found:

$$\frac{Q}{\frac{1}{2}\pi R^3 \rho U_{rated}^2} = \frac{P \cdot U_{rated}}{\frac{1}{2}\rho A U_{rated}^3 \cdot \Omega R} \tag{9}$$

which can be simplified to:

$$Q = \frac{P}{\Omega} \tag{10}$$

Since Ω is constant, the torque and power capacity are linearly correlated.

3.2.4 Design driver: Gravity force

The gravity force is described as:

$$F_g = m \cdot g \tag{11}$$

Here, F_g is the gravity force, m is a mass and g is the gravitational acceleration. The gravity force is not a constant force throughout the turbine, since it only uses masses of components that need to be supported by another component. The mass (and therefore the gravity force) of not all components is scaled. The yaw system, pitch system, shaft, controller system, bearings, miscellaneous components, battery and fuel cell are not scaled. The reasoning behind this is given below in the components' relevant parts of section 3.3. Since the gravity force is different for different components it affects, the components included for the relevant gravity forces can be seen in table 2. As can be seen, some components are not needed for scaling with gravity force. Since the mass of those components is not necessary for the gravity force, nor for the determination of the cost of the component, the masses can be ignored in this model.

Table 2: Components (vertical) included in the gravity force acting on relevant components (horizontal)

Component	**Tower**	**Hub**	**Bedplate**
Electrolyser system			
Compressor			
Converter system	X		
Generator	X		X
Blades	X	X	X
Hub	X		X
Bedplate	X		
Tower			
Transition piece			
Monopile			
Battery			
Fuel cell			
Yaw system	X		
Pitch system	X		
Bearings	X		
Shaft	X		
Miscellaneous components	X		
Controller system	X		

3.3 Modelling of component scaling

In this section, the components as seen in table 1 are discussed. The section will describe how the above given drivers are used in the scaling and modelling of each component.

3.3.1 Electrolyser system

The basis for the electrolyser system scaling is the idea that an increasing rated power can simply be dealt with by adding extra stacks to the electrolyser. The water purification systems are assumed to scale linearly with the increasing electrolyser stack amount, since more stacks require more purified water. The water purification system is also included in the electrolyser system cost. Therefore, from a price per kilowatt starting point, the cost of the electrolyser system can be determined for every change in power capacity.

The price is set at 300 €/kW, which is based on information provided by HYGRO and their supplier Plug-Power, validated by comparing it to data by NREL [23]. Within this NREL report, figure 8 is given. Here the expected cost of a normal electrolyser system is given for different annual production rates in steps of megawatts. The scope of this model is around 1,000 MW. Therefore, at an annual production rate of 1,000 units of 1 MW, a cost of around 300 $/kW is found. Converting this to euros leads to a price of 255 €/kW. It should be noted that this price does not include all components of the electrolyser system, such as the water purification which would increase the final price. It should also be noted that the increase from 1,000 annual units to 2,000 units does not result in a large decrease in price. This means that if the power capacity is doubled from the original scope of 1,000 MW, the change in electrolyser price is minimal. Based on these two points, the expected cost provided by HYGRO and their supplier can be assumed reasonable, resulting in equation 12, with $C_{electrolyser}$ as the electrolyser cost.

$$C_{electrolyser} = P_{rated} \cdot 300 \text{ [€/kW]} \tag{12}$$

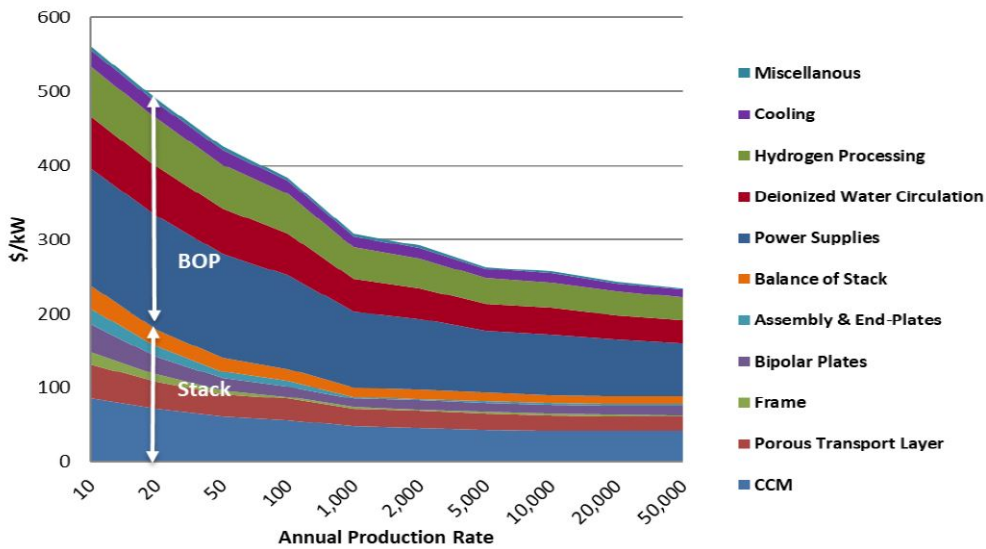

Figure 8: System cost [$/kW] - PEM - 1 MW [23]

3.3.2 Compressor

The piston compressor system is assumed to scale with the increasing size of the electrolyser, since a larger electrolyser system results in more hydrogen that needs to be compressed to 100 bar. Since the electrolyser scales with power, the compressor does so as well. Through HYGRO supplier Howden Compressors, the cost function as can be seen in equation 13 is found, where $C_{compressor}$ is the compressor cost.

$$C_{compressor} = 100,000 + P_{rated} \cdot 48 \text{ [€/kW]} \tag{13}$$

3.3.3 Converter system

A converter system's size and cost are dependent on how much power it will need to process. Because of this, the converter cost is determined as a function of power capacity. The relation between the cost and power capacity has been set at 79 $/kW by NREL in 2006 [24]. Conversion to 2020 dollars results in a cost of 114.34 $/kW or 97.19 €/kW, as explained in section 3.1. In order to validate this, it is compared to the cost found in a report by BVG Associates for The Crown Estate in 2019 [20]. Here, a cost of £700,000 or €805,000 is given for a 10 MW wind turbine converter system in the section Power take-off. Converting this to a cost per kW results in 80.5 €/kW. The difference between the two values can be explained by improvements in technology between the release of both data. By taking the average of the combined values in a ratio of 1:2 (NREL:BVG), a cost per kW is set at 86.06 €/kg. The heavier emphasis on the cost of the BVG converter system is used to account for the fact that the information of BVG is more current and therefore has taken into account innovations in technology.

Both the cost of NREL and BVG are for a normal wind turbine. BVG describes it in their report as a power converter, transformer, switchgear and cables. Most of these components are not relevant for a hydrogen turbine, as described in chapter 2. In order to compensate for this, in consultation with HYGRO, it was decided that ignoring 60% of the costs of the power take-off is a reasonable estimate for the cost of the converter system in the hydrogen turbine. By subtracting 60% of the cost, a final cost is set at 34.43 €/kW. The function of converter system cost to power capacity is therefore found in equation 14.

$$C_{converter\ system} = P_{rated} \cdot 34.43 \text{ [€/kW]} \tag{14}$$

The mass of the converter system is based on information of the ACS880 converter by ABB [25]. Here, the mass of relevant AC/DC converters is given for a range between 0.8 and 8 MW. A linear fit through these masses results in equation 15, where $m_converter$ is the converter mass in kg and P_{rated} is in kW. It is assumed that this equation for the mass is also relevant for converters of sizes larger than 8 MW, since the 8 MW ACS880 converter by ABB is described as a combination of two 4 MW converters, therefore alluding to the possibility of simply adding a converter if necessary.

$$m_{converter} = 0.9618 \cdot P_{rated} + 171.5 \tag{15}$$

3.3.4 Generator

The base cost of the generator is based on earlier defined scaling laws as well as a current cost of a direct-drive generator. The in 2006 determined scaling laws [24] state a linear relation between the cost and power capacity. Here, a cost of 219.33 $/kW in 2002 USD is given. To convert this to 2020 USD, the same method as for the converter system is used. This results in a cost of 317.33 $/kW [26], or around 270 €/kW. Since the report by NREL can be outdated due to its publication date, it is compared to a cost per kW of a more recent direct drive generator. Within the previously mentioned report by BVG associates, it is stated that "The direct drive generator cost for a 10MW wind turbine is over £2 million." [20], which is equal to 200 £/kW. Converted to euros, this leads to a price of at least 230 €/kW. Combining both values and keeping in mind that the cost determined by BVG Associates is a minimum, an average cost of 250 €/kW is chosen.

Since the size of the generator could increase to a size twice that of currently produced turbines, a factor is added in order to increase the cost of the generator to a higher level at high power capacities. This is described in equation 16.

$$C_{generator,\ new} = (\frac{P_{new}}{P_{ref}})^{\Xi} \cdot P_{ref} \cdot 250 \text{ [€/kW]} \tag{16}$$

Here, C is the cost, P is the power rating and Ξ is the factor.

The mass of the direct-drive generator scales with the rated torque in the low-speed shaft, according to scaling correlations found by NREL [27]. This correlation is given in equation 17,

$$m_{generator} = 172.8 \cdot (Q_{LSS})^{0.8} \tag{17}$$

where $m_{generator}$ is the generator mass in kg and Q_{LSS} is the low-speed shaft rated torque in kNm.

3.3.5 Pipeline

As described in section 2.2.5, the pipeline used is a High Pressure Flexible Composite Pipe Systems by SoluForce [17]. The cost per unit of power of the wind farm and per unit of pipeline length is determined using information supplied by HYGRO and set at 1.25 €/(kW · km). This cost level is based on internal information of HYGRO from their supplier SoluForce. Here the relevant power for the pipeline is the power of the entire wind farm. Equation 18 describes the correlation, where $C_{pipeline}$ is the pipeline cost, P_{rated} is the combined rated power of all turbines in the wind farm and L_{shore} is the distance to shore from the wind farm.

$$C_{pipeline} = P_{rated} \cdot L_{shore} \cdot 1.25 \text{ [€/(kW · km)]} \tag{18}$$

3.3.6 Blades

Under normal conditions, the blade design is driven by a combination of different forces. This designing normally includes changes in thickness of the blades, but also in the geometry. However, since this model reviews a large number of different turbine designs, it was decided to only calculate the changes in mass of the blades when the power capacity is increased. Furthermore, no changes in the aerodynamic design and thus in exterior geometry are made. Therefore, the increase in mass is achieved by adding material inside the blade. The new mass is multiplied with an average cost per unit mass of the blades that includes production cost. This method also ignores differences in amounts of added material types and assumes that the cost per unit mass of the blade is constant.

The main goal of the blade design is to keep the stresses inside the blade constant. The main stresses in the blade are a result of the force acting on the blade. Figure 9 depicts a cross section of a typical section of the blade along with the forces acting on it. As can be seen, the normal force F_n is acting perpendicular to the plane of rotation and can thus be linked to the thrust acting on the wind turbine. The tangential force F_t is a force that contributes to the torque. The torque is the integration of the force F_t multiplied by the lever arm. The lever arm in this case is the location on the blade that F_t is acting on. It can be seen clearly that the size of the thrust is much larger than that of the torque. Furthermore, the resistance against bending in the flapwise direction is lower than in the edgewise direction. Therefore, the design in most of the blade is driven by the thrust and in the strengthening of the blade in the flapwise direction.

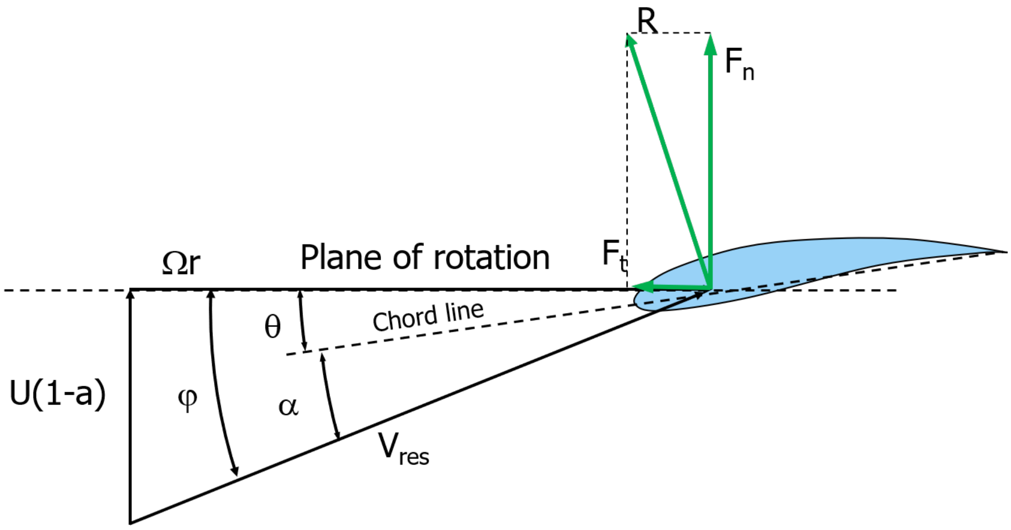

Figure 9: Cross section of a blade along with the forces acting on it [19]

The thrust is normally compensated through strengthening the blade. This is done by increasing the size of the shear webs and spar caps, since these are more relevant to the resistance in the flapwise direction. The necessary increase in strength to compensate for the torque is achieved by increasing the size of the leading and trailing edge panels of the blade. The location of all these parts of the blade are given in figure 10.

The stress that occurs as a result of the thrust is the bending stress. Therefore, the dominant stress on most sections of the blade is the bending stress. Equation 19 is derived to calculate the bending stress $_{bend}$.

$$\sigma_{bend} = \frac{My}{I} \tag{19}$$

Here, M is the moment, y is the perpendicular distance to the neutral axis and I is the area moment of inertia. The moment here is a result of the thrust acting on the blades. The thrust increases with higher power capacities, as described in section 3.2.2. This will result in a proportional increase in moment. Since the bending stress needs to be kept constant, the terms y and I need to compensate for this. Since decreasing

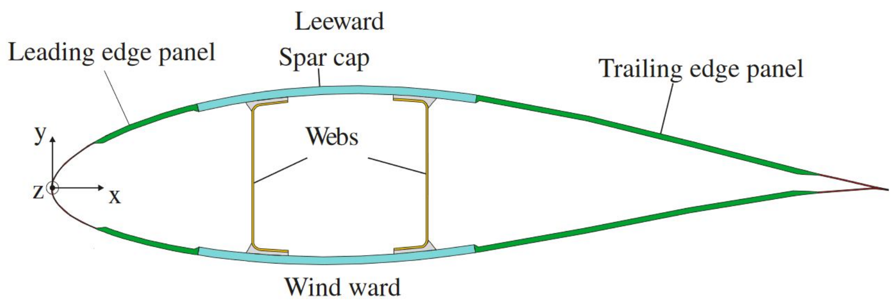

Figure 10: Cross section of wind turbine blade section [28]

the perpendicular distance to the neutral axis to compensate for an increase in moment is not an option due to the choice of an unchanged aerodynamic design, the increase in moment is compensated with the area moment of inertia.

The simplest method to increase the area moment of inertia is by using a thickness factor. A thickness factor is an uniform increase in the thickness of the blade skin, spar caps and shear webs, without changing the outer design of the blade. Therefore, the main dimensions such as the chord and the airfoil thickness remain the same.

The area moment of inertia is defined as:

$$I = \int_A p^2 dA \tag{20}$$

where p is the perpendicular distance of dA from the neutral axis. Since the exact area moment of inertia of each blade section can not be determined, the blades need to be approached differently. All blade elements, such as the spar caps and webs remain in the same position. When the blade is approached as a thin shell, the blade can be deconstructed with line element with length dl and thickness t, as seen in equation 21.

$$dA = t \cdot dl \tag{21}$$

When a thickness factor t_f is introduced, equation 21 can be rewritten as:

$$dA_f = t_f \cdot t \cdot dl = t_f \cdot dA \tag{22}$$

Since the blade elements are approached as thin shelled, thickness t will be small. Therefore, a change in thickness does not have an effect on the position of the line element and therefore doesn't affect distance p either. By including the thickness factor, I can be rewritten as equation 23

$$I_f = \int_A p^2 dA_f = \int_A p^2 \cdot t_f \cdot dA = I \cdot t_f \tag{23}$$

By rewriting equation 19, the following correlation is found:

$$\sigma_{bend} = \frac{M_{ref} \cdot y}{I_{ref}} = \frac{M_{new} \cdot y}{I_{new}} = \frac{M_{new} \cdot y}{I_{ref} \cdot t_f} \tag{24}$$

Therefore:

$$\frac{M_{new} \cdot y}{M_{ref} \cdot y} = \frac{M_{new}}{M_{ref}} = \frac{I_{ref} \cdot t_f}{I_{ref}} = t_f \tag{25}$$

The moment is the sum of different thrust components dT multiplied by their respective lever arm. Since the position of the thrust components do not change in the blade, the moment is only dependent on the thrust. Therefore, equation 25 can be rewritten as:

$$t_f = \frac{T_{new}}{T_{ref}} \tag{26}$$

where T is the thrust.

As stated above, for most blade sections, thrust is the dominant design driver, which is compensated by the thickness factor affecting the size of the shear webs, spar cap and skin. However, the torque also has an effect on the blade design, which needs to be compensated by increasing size of the leading and trailing edge panels.

For the purpose of estimating the change in mass of the blade, the thickness factor is assumed to result in a blade strong enough for both the increased thrust and torque. This is assumed since the spar caps and shear webs are large and already have a higher mass than the other parts such as the leading and trailing edge panels. Therefore, when the mass of the spar caps and shear webs is increased through a thickness factor, this will result in a large increase in mass in the entire blade. In the areas where the torque is dominant and thus the leading and trailing edge panels need to become larger, the spar caps and shear webs do not need to be strengthened as much. Therefore, the extra mass available for the spar caps and shear webs would likely be enough to strengthen the leading and trailing edge panels there, making the blade strong enough for both thrust and torque.

Since the geometry of the blade is not changed in this model, the blade design is not optimal. An actual blade design will likely not only compensate higher forces through extra material, but also through a different aerofoil design that handles the forces better. Furthermore, as stated above, the strengthening through extra material in the places where torque is dominant is done by using material not needed for thrust compensation there. The amount of mass available for thrust compensation is likely to be higher than what is needed for the torque compensation, since the spar caps and shear webs are larger and therefore have more mass added due to the thickness factor. Because of both these reasons, the thickness factor likely leads to an overestimation of the blade mass. To compensate for this overestimation, a correction factor X is used. This correction factor decreases how quickly the thickness factor increases with increasing power capacity.

The new blade cross-sectional area defined by the thickness factor linearly correlates to an increase in volume, due to the constant blade length. This increase in volume is assumed to result in a linear increase in mass, since all different parts of the blade element increase uniformly and no distinction is made between the materials used. Therefore, the blade mass is described as:

$$m_{blade,\ new} = m_{blade,\ ref} \cdot (t_f^X) \tag{27}$$

where m_{blade} is the blade mass of a single blade, t_f is the thickness factor and X is the correction factor.

The blade costs per unit mass include all costs, such as manufacturing, materials and labour. The cost per mass is set at 14.6 €/kg. This price is based on information in the aforementioned report by BVG, where is stated that "The set of blades for a 10MW wind turbine costs about £1.3 million." [20]. These blades are also stated to have a total mass of 90-120 tonnes, The £1.3 million converted results in €1.5 million. These costs are associated with blade materials including fibreglass, epoxy and polyester resins, and carbon fibre [20]. By comparing the cost with the mass, a final cost between 12.5 and 16.7 €/kg is found, with an average of 14.6 €/kg. This cost is multiplied with the earlier found new blade masses to determine the cost of the blades for each power rating.

Since the model does not make a distinction between the different materials in the blade, the mass is multiplied with the cost per unit mass to determine a blade cost. The expected blade cost equation can be seen in equation 28.

$$C_{blades} = (m_{blade} \cdot 3) \cdot 14.6 \text{ [€/kg]} \tag{28}$$

Here, C_{blades} is the cost of all three blades.

3.3.7 Hub

The hub mass scales with the blade mass. The relation between blade mass and hub mass is determined by NREL [24] in 2006. Here, a linear relation between the hub mass and the blade mass is deduced. This relation has been re-calibrated using the mass of two other hub masses. The hubs used are from the 15 MW and 10 MW IEA reference wind turbines [8] [29]. The hub of the 15 MW turbine has a mass of 190,000 kg, while the hub of 10 MW turbine weighs 81,700 kg. Comparing these to the blade mass of both turbines (65,300 kg and 47,700 kg respectively), a linear relation is determined. The cost associated with this mass is based on the 50,000 kg and £150,000 hub in the 10 MW turbine discussed by BVG Associates [20]. These values result in a cost of 3 £/kg or 3.45 €/kg. The linear relation and cost are combined in equation 29, where C_{hub} is the cost of the new hub, while m_{blade} is the mass of a single blade.

$$C_{hub} = (6.171 \cdot m_{blade} - 212,600) \cdot 3.45 \text{ [€/kg]} \tag{29}$$

3.3.8 Bedplate

The bedplate scales linearly with the increasing mass it has to support. This mass is described by the ratio of the new and original mass of the hub, blades and generator. By multiplying the original bedplate mass with this mass factor, a new bedplate mass is determined. The cost is based on the report *WindPACT Turbine Rotor Design Study* by NREL. Here, a cost for a bedplate is given as 4.25 \$/kg in 2002 USD [30], or 6.15 \$/kg in 2020 USD. Converted to euros this results in a cost of 5.23 €/kg. The bedplate mass and cost per unit mass are combined in equation 30, where $C_{bedplate}$ is the cost of the bedplate and the different m variables are the masses of specific parts.

$$C_{bedplate} = (m_{bedplate,\ ref} \cdot \frac{m_{hub,\ new} + m_{blade,\ new} \cdot 3 + m_{generator,\ new}}{m_{hub,\ ref} + m_{blade,\ ref} \cdot 3 + m_{generator,\ ref}}) \cdot 5.23 \text{ [€/kg]} \tag{30}$$

3.3.9 Tower

Mass determination of tower

The scaling of the tower is based on three principles. The first is keeping a constant bending stress, the second is a constant compression stress and the third is avoiding buckling. These are chosen to roughly try to keep the tower design resilient to the forces acting on it. The tower designs determined in this model are only based on static conditions and are therefore imperfect.

It is important to note that both stresses have a different effect on different areas of the tower. The bending stress affects the bottom of the tower more than the top, due to the moment present in the definition of the bending stress. This moment is defined by the height of the tower as the arm multiplied with the force acting on the tower. This force is taken as the thrust, which is considered the dominant force. This means that the top of the tower will have a minimal arm, so a minimal bending stress, while the bottom of the tower uses the entire height of the tower as its arm. On the other hand, the compression stress has lower overall values than the bending stress. Both these conditions mean that at the bottom of the tower, the stresses are dominated by the bending stress, while the top is dominated by the compression stress.

The method chosen to avoid buckling is keeping the ratio between the wall thickness and the diameter constant. However, the top of the tower needs to maintain a constant tower diameter, since the yaw system is not redesigned but still needs to fit. In order to solve this, a compromise needs to be made. Therefore, the constant ratio between the wall thickness and tower diameter is not applied at the top of the tower, where only the wall thickness can increase, but the diameter remains constant.

Since aiming to keep both of the stresses constant throughout the tower is not a realistic goal, a combination of both is necessary. In order to achieve this, a new tower diameter and wall thickness for the bottom and a wall thickness for the top of the tower are determined. As stated before, the bending stress dominates the bottom of the tower, while compression stress dominates at the top. Therefore, the diameter and thickness at the bottom are calculated in a situation where only the bending stress is present, while the thickness at the top is calculated as a result of only compression stress. Since the ratio between the wall thickness and diameter is kept constant for the bottom of the tower, the increase in wall thickness at the bottom is the same as the increase of diameter. The new wall thicknesses at the top and bottom are compared to a reference tower dimensions. This comparison results in factors f_b and f_c, where f_b is the factor at the bottom, while f_c is the factor at the top, as seen in equation 31 and 32.

$$f_b = \frac{t_{w,\ bot\ new}}{t_{w,\ bot\ ref}} \cdot f_u - (f_u - 1) \tag{31}$$

$$f_c = \frac{t_{w,\ top\ new}}{t_{w,\ top\ ref}} \cdot f_u - (f_u - 1) \tag{32}$$

Here, t_w is the wall thickness and f_u is an uncertainty factor that is comparable to a thickness factor and increases the factors f_b and f_c.

The factors f_b and f_c are used to calculate the new wall thickness and tower diameter throughout the tower at several different height levels z'. This dimensionless z' is defined as:

$$z' = \frac{z(i)}{h} \tag{33}$$

where $z(i)$ is a height coordinate for point i in the tower and h is the height of the tower. Equation 34 and 35 give the calculation for the new wall thickness and diameter at point z', which correlates to a specific point in the tower.

$$t_w(i) = t_{w,\ ref}(i) \cdot (z' \cdot f_c + (1 - z') \cdot f_b) \tag{34}$$

$$D(i) = D_{ref}(i) \cdot (z' + (1 - z') \cdot f_b) \tag{35}$$

These dimensions at different sections i in the tower are used to calculate the cross-sectional area of those sections using equation 36.

$$A(i) = \pi \cdot ((\frac{D(i)}{2})^2 - (\frac{D(i) - 2 \cdot t_w(i)}{2})^2) \tag{36}$$

These areas are combined with the height coordinate z of relevant section i minus the height coordinate z of the section below i to calculate the sectional volume. These volumes are added together to calculate the new volume of the tower, as seen in equation 37.

$$V_{new} = \sum_{i=2}^{max\ i} A(i) \cdot (z(i) - z(i-1)) \tag{37}$$

The next two sections describe how the outer diameter and wall thickness for the top and bottom are calculated

Bending stress tower

Equation 19 is used to calculate the bending stress σ_{bend}. Here, M is the moment, y is the perpendicular distance to the neutral axis or the centre of the tower and I is the area moment of inertia. The moment M is defined by the thrust on the tower multiplied by the distance to the section where the thrust vector points at. The perpendicular distance to the neutral axis is in this case equal to the radius of the tower. The area moment of inertia is defined in equation 38.

$$I = \pi \cdot \frac{D_{outer}^4 - D_{inner}^4}{64} \tag{38}$$

Where D_{outer} is the outer diameter of the tower and D_{inner} is the inner diameter. The inner diameter can also be described as:

$$D_{inner} = D_{outer} - 2 \cdot t_w \tag{39}$$

where t_w is the wall thickness. Since the wall thickness to diameter ratio is kept constant in order to avoid buckling when the design is driven by bending stress, the wall thickness can be described as:

$$t_w = D_{outer} \cdot \Theta \tag{40}$$

where Θ is the ratio between the wall thickness and outer diameter. From these equations, the inner diameter can be rewritten as:

$$D_{inner} = D_{outer} - 2 \cdot D_{outer} \cdot \Theta \tag{41}$$

The rewritten form of the inner diameter can be used in the area moment of equation 38 as equation 42.

$$I = \pi \cdot \frac{D_{outer}^4 - (D_{outer} - 2 \cdot D_{outer} \cdot \Theta)^4}{64} \tag{42}$$

When the power rating of the wind turbine increases, the thrust will increase as well, as seen in section 3.2.2. This increase will therefore also increase the moment on the bottom of the tower. Since the bending stress σ_{bend} should be kept constant, the $\frac{y}{I}$ term will have to compensate the thrust increase. By rewriting the definition of σ_{bend} to isolate D_{outer}, equation 43 is derived.

$$D_{outer} = \sqrt[3]{\frac{T \cdot h \cdot 64}{\sigma_{bend} \cdot 2 \cdot \pi \cdot (1 - (1 - 2 \cdot \Theta)^4)}} \tag{43}$$

Here T is the thrust and h is the distance to the top of the tower. Using this equation, the outer wall diameter can be determined for different thrust values, which themselves are a result of different power capacities. The outer diameter can also be used to determine the wall thickness based on the earlier defined constant Θ as seen in equation 40.

Compression stress tower

Equation 44 is derived to calculate the compression stress σ_{comp}.

$$\sigma_{comp} = \frac{F}{A} \tag{44}$$

Here, F is the force acting on area A. At the top of the tower, F is the gravitation force of the mass of the components on top of the tower multiplied by the gravitational acceleration and A is defined by equation 36. The mass relevant at the top of the tower is that of the rotor-nacelle assembly. The components that are therefore included are: blades, bearings, yaw and pitch system, generator, converter system, hub, bedplate, controller system and the miscellaneous components. At the top of the tower, the yaw system is a limiting factor for the size of the outer diameter. Therefore, the outer diameter is a constant. When the power rating of the turbine increases, it will affect several components' masses, such as the generator and the blades. This increased mass will change the F in equation 44. In order to keep the compression stress constant, the area A will have to increase as well to compensate for the increased mass. This increase in area is achieved by increasing the wall thickness, since the outer diameter is kept constant. By rewriting the compression stress equation, the wall thickness can be isolated and defined as stated in equation 45,

$$t_w = \frac{D_{outer}}{2} - \sqrt{(\frac{D_{outer}}{2})^2 - \frac{F_{g,\ tower}}{\pi \cdot \sigma_{comp}}} \tag{45}$$

where $F_{g,\ tower}$ is the gravity force of the relevant components as described in section 3.2.4.

Cost of the tower

The cost of the tower is based on a price per unit mass. This mass itself is dependent on the increase in volume, since the density of the tower is considered constant. As described above, the new tower volume is calculated using equation 37. These volumes can be used in equation 46 to determine tower mass m_{tower}.

$$m_{new} = \frac{V_{new}}{V_{ref}} \cdot m_{ref} \tag{46}$$

In cost per unit mass is based on the 10 MW turbine described in the aforementioned report by BVG Associates. Here, a tower with a mass of 600,000 kg is priced at £700,000 or €815,000 [20]. From these values, a cost of 1.36 €/kg is found, which is multiplied with the new found tower masses for each power rating as can be seen in equation 47.

$$C_{tower} = m_{tower} \cdot 1.36 \text{ [€/kg]} \tag{47}$$

3.3.10 Transition piece

The transition piece scaling is done similarly to that of the tower, with some important exceptions. Firstly, the tower diameter is not limited by the yaw system. Therefore, it is allowed to increase with the power rating. Secondly, buckling is here kept as relevant for the entire transition piece, resulting in ratio Θ between D_{outer} and t_w as seen in equation 40. This results in this ratio being applicable at all heights of the transition piece. Thirdly, the design is only driven by the bending stress. Since within the tower, at the bottom the design is already completely dominated by the bending stress, it is assumed that in the transition piece below the tower, the bending stress will also be the dominant stress.

In order to determine new dimensions of the transition piece, the dimensions at the bottom are calculated, similar to that of the tower. The dimensions at the bottom of the transition piece are dependent on the bending stress. Therefore, equation 43 can be re-used to calculate the diameter and by using Θ, the thickness can be calculated. The new wall thickness is used in equation 31 to determine a factor f_b. One difference here, is that the factor f_u can be set separately for the transition piece. f_b is then used in equation 48 and 49 to determine the dimensions for each section i.

$$t_w(i) = t_{w,\, ref}(i) \cdot f_b \tag{48}$$

$$D(i) = D_{ref}(i) \cdot f_b \tag{49}$$

Using equation 36, the area for each section i is calculated. These areas are used in equation 37 to calculate the new volume of the transition piece.

Comparable to the tower, the transition piece mass is determined using equation 46. The cost of the transition piece is next determined using a price per mass. This price is based on the 10 MW turbine discussed in the report by BVG Associates. Here, the transition piece has a mass of 500,000 kg and a cost of £1 million or €1,150,000 [20]. Rewritten, this results in a cost of 2.3 €/kg. Equation 50 describes how the cost is calculated.

$$C_{transition\ piece} = m_{transition\ piece} \cdot 2.3 \text{ [€/kg]} \tag{50}$$

3.3.11 Monopile

The monopile scaling is split up into the scaling above the sea-bed and below it. For the part above the sea-bed, the buckling is the most important variable to keep constant. The reference monopile is designed with the buckling effects resulting from pile driving in mind. Therefore, the ratio between wall thickness and diameter will be kept constant from this reference turbine. The other important aspect for monopile design is the bending stress, which should be kept constant as well. Based on these two boundary conditions, equation 43 can be used again to calculate the outer diameter. From this diameter and the ratio between the wall thickness and the diameter, the wall thickness can also be determined. These dimensions are, in a similar way to the transition piece, used to determine the outer diameter and wall thickness of each section of the monopile above the sea-bed. With these sectional dimensions, the area of each section is calculated with equation 36. Multiplying these areas with the respective section height will result in several volumes that are combined to determine a new monopile volume above the sea-bed.

The monopile has a constant area for the entire section below the sea-bed. This area is the same as that of the area just above the sea-bed, as calculated above, and is a result of the bending moment. However, the embedment depth of the monopile is also needed to determine the volume of the sub-sea-bed monopile. The critical embedment depth is calculated according to Blum's method [31] [32]. This method allows for two conditions where either the moment or the force acting on the top of the pile is dominant. The moment acting on top of the pile is also known as the overturning moment. Both the moment and force used are a result of the thrust acting on the turbine. The force is the same as the thrust and the overturning moment is the thrust multiplied by the height of the turbine above the sea-bed. Both conditions are given in equation 51 (embedment depth dominated by the overturning moment) and equation 52 (embedment depth dominated by the force acting on the top of the pile).

$$h_{pile,\, F=0} = \sqrt[3]{\frac{|M_{overturning}|}{C_M \cdot D}} \tag{51}$$

$$h_{pile,\ M=0} = \sqrt{\frac{|T_{pile\ top}|}{C_F \cdot D}} \tag{52}$$

Here, h is the embedment depth of the monopile, $M_{overturning}$ is the overturning moment, C_M and C_F are constants that can be determined by using the embedment depth of a reference turbine and either the force or the moment set to zero, D is the monopile outer diameter and $T_{pile\ top}$ is the thrust acting on the top of the turbine. Both equations will give different monopile embedment depths. Within this model, it is assumed the overturning moment is dominant. Therefore, equation 51 is used to calculate the depth. Factor χ replaces the cube root in this equation. This factor is used to adjust for uncertainties in the domination of the overturning moment. Depending on the value of χ, the embedment depth can be adjusted to approach a situation where the overturning moment is an over- or underestimation. Equation 53 gives the final equation used to calculate the embedment depth of the monopile. Here, χ has a standard value of three.

$$h_{pile} = \sqrt[\chi]{\frac{|M_{overturning}|}{C_M \cdot D}} \tag{53}$$

The determined embedment depth is multiplied with the earlier calculated area at the bottom of the monopile just above the sea-bed. This will yield the volume of the monopile below the sea-bed.

Lastly, the different volumes of both the top and bottom of the monopile are added. This total volume is compared to the volume of the reference monopile. The factor by which the volume is increased is multiplied with the original monopile mass to determine a new monopile mass.

The cost of the monopile is again determined by the cost per mass as found in the report by BVG Associates. Here, the 10 MW turbine has a monopile with a mass of 2,000,000 kg and a price of £1.5 million or €1.725 million [20]. This results in a cost of 0.8625 €/kg, as seen in cost equation 54.

$$C_{monopile,\ new} = (m_{monopile,\ ref} \cdot \frac{V_{monopile,\ new}}{V_{monopile,\ ref}}) \cdot 0.8625 \text{ [€/kg]} \tag{54}$$

3.3.12 Installation of turbine and pipeline

Both the turbine installation and pipeline installation are kept constant, since the increasing power would result in changes within the turbine itself and the size of the pipeline, but barely in the installation cost. A heavier turbine with a higher power rating is assumed not to result in the need for much more expensive or complex installation methods. The main drivers for such increases are the hub height and rotor diameter, which are both kept constant. The same can be said for the pipeline installation, where the cost for laying a bigger pipe is assumed to result in a small and limited increase in cost. It should be noted that the turbine installation includes the foundation and monopile, while the pipeline installation is stated per kilometer of pipeline necessary. Both costs are based on information by BVG [20] and can be seen in table 3. Here, the turbine installation cost is based on the cost of one hundred 10 MW turbines and includes the monopile transport and installation as well as the turbine transport and installation onto the monopile. The cost was normalised per turbine by dividing this total cost by one hundred to obtain a cost per turbine. The installation cost of the pipeline is assumed to be the same as the offshore cable installation described by BVG, where the installation is assumed to be for a 60 km offshore location. Therefore, the total cost is divided by the 60 km to determine a cost per kilometer. The offshore cable installation includes the cable lay, burial and pull-in as well as testing. The cost of the pipeline installation is assumed to be the same, since it requires most of the same costs. The pull-in of the cable is not required for the pipeline, so this cost is subtracted from the total.

Table 3: Overview of costs of wind farm components

Component	**Cost [€]**
Installation turbines	1,725,000/turbine
Installation pipeline	4,083,333/km

3.3.13 Decommissioning, operations and maintenance of a wind farm

The decommissioning, operations and maintenance are assumed to be constant, independent of the power capacity of the turbines on the wind farm. However, since all three of these costs are incurred later in the project, they are discounted, as described above in section 3.1 in equation 2. The decommissioning cost is paid at the end of the wind farm's lifetime. The operations and maintenance costs are yearly costs, so are discounted yearly. The decommissioning cost is based on the report by BVG [20]. It includes one hundred 10 MW turbines, the foundation and the cable decommissioning, where the cost of the pipeline decommissioning are assumed the same as the cable decommissioning. The cost is normalised per turbine by dividing the total decommissioning cost by the 100 turbines it is relevant for. The operations costs include training, health and safety inspections, offshore logistics and onshore logistics. The maintenance costs include turbine maintenance and service, as well as balance of plant maintenance and service. Both are also based on the same report by BVG [20]. Table 4 stating the costs of all three in their undiscounted form.

Table 4: Overview of costs of wind farm components

Component	**Cost [€]**
Decommissioning of wind farm	2,875,000/turbine
Operations	28,750,000/year
Maintenance	57,500,000/year

3.3.14 Battery and fuel cell

Since both the battery and fuel cell only need to supply power in case of failure or for start-up, the amount needed is independent of the power rating of the turbine. Therefore, both are kept constant. Their masses also are not needed for further modelling, so both have not been determined. The data on the battery has been provided to HYGRO by NREL and the fuel cell was provided in a similar way by PlugPower. Since the batteries and fuel cell are not dependent on the rated power, these costs are constant for a wide range of power capacities. The cost of the battery and fuel cell are €5,000 and €20,000, respectively.

3.3.15 Yaw and pitch system shaft and main bearings

The yaw system is one of the components with a constant cost. During normal turbine design, it is scaled with the rotor diameter [24]. However, since the rotor diameter is kept constant, no scaling is applied. The pitch system and shaft are approached in the same way, since they also scale with the rotor diameter. The main bearings are also scaled with the rotor diameter, as described by NREL in a WindPACT report [30]. Therefore, their costs are kept constant. Since they are not scaled, their mass is also kept constant, as stated before in section 3.2.4.

The costs are based on the technical report by BVG [20]. Here, a yaw system for a 10 MW turbine costs €276,000 and includes the yaw motors, brakes, bearings and sensors. Since the yaw system cost is associated with the rotor diameter, the cost is divided by the rotor diameter. The rotor diameter of the turbine used by BVG is 193 meters. Therefore, a cost of 1430 euros per length unit of rotor diameter is used. The pitch system cost for a 10 MW turbine with a rotor diameter of 193 meters is €115,000, or 596 euros per length unit of rotor diameter. The shaft cost of €230,000 is also based on the shaft of a 10 MW turbine as described by BVG [20]. Since the shaft size is also based on the rotor diameter, the same method as for the yaw system is applied. This results in a cost of 1,192 euros per length unit. Lastly, the main bearings cost is approached in the same way. Here, the cost of the main bearings for a 10 MW, 193 meter rotor diameter turbine is €230,000 or 1,192 €/m. In order to determine the cost of these components during modelling, the rotor diameter of the chosen reference turbine is multiplied with the costs per length unit as seen below in table 5.

Table 5: Cost per unit length of the rotor diameter for the yaw and pitch system, the shaft and the main bearings

Component	Cost [€/m]
Yaw system	1,430
Pitch system	596
Shaft	1,192
Main bearings	1,192

3.3.16 Miscellaneous components and controller system

The miscellaneous components, including fasteners, small engineering components, nacelle cover, spinner and the rotor and nacelle auxiliary systems, are kept constant as well. All these components are assumed to be constant with an increasing power due to the very minimal scaling that would occur with an increasing power rating. The controller system is kept constant, since changing the power capacity does not affect how the controller system functions. The cost of the miscellaneous components is based on the report by BVG [20]. Here, the cost of all components included in the miscellaneous components as well as the cost of the controller system are from a 10 MW turbine. These costs are assumed to be representative for larger turbines as well. The cost of the miscellaneous components is €586,500 and of the controller system is €287,500.

3.4 Production

3.4.1 Determination of production level

The annual production of hydrogen is based on the hydrogen production curve of a hydrogen turbine. An example of the steps taken to make such curve is given here in figure 11 for a 15 MW turbine, of which the (electrical) power curve is known. This power curve is converted to a hydrogen production power curve by HYGRO, based on measurements from an external model description [33]. The 15 MW hydrogen production power curve resulting from this can be seen in figure 12. The efficiency of the hydrogen production is plotted within this figure as well. This efficiency describes how much energy is lost in the production of hydrogen compared to the generator output. It includes all losses after the generator up to the point where the hydrogen has been created. As can be seen, the efficiency is higher at lower wind speeds. Since PEM electrolysers have a higher efficiency at low power, this higher efficiency is prolonged as long as possible by turning on electrolyser stacks as soon as enough power is available for the extra stack. At rated power, all electrolyser stacks are turned on and therefore, the efficiency is stabilised.

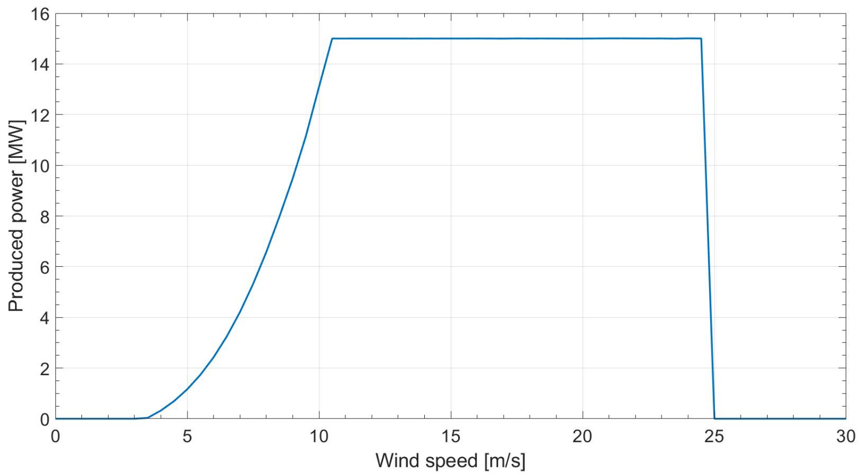

Figure 11: Power curve for a 15 [MW] wind turbine

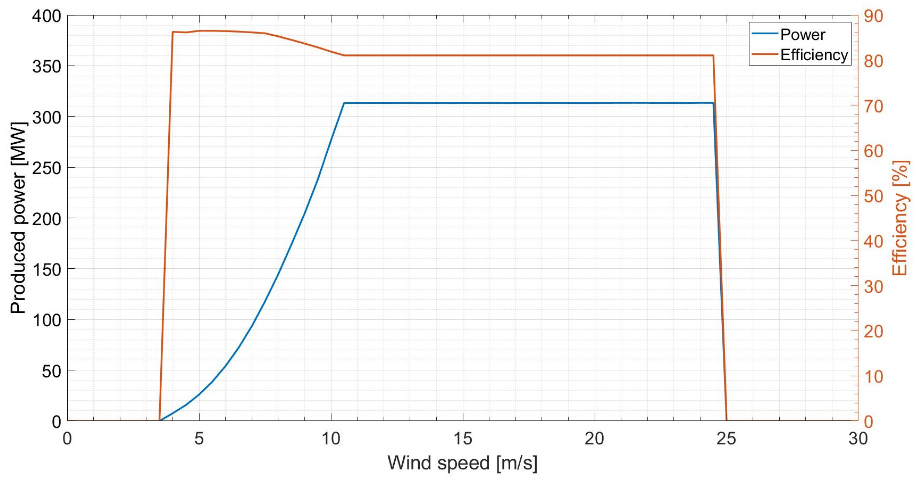

Figure 12: Hydrogen production curve for a 15 [MW] hydrogen turbine, supplied by HYGRO

In order to convert these production curves to actual amounts produced, Weibull data is used for the relevant location. The Weibull parameters were used to determine the Weibull probability density function as seen in equation 55.

$$f(U) = \frac{k}{a} \cdot (\frac{U}{a})^{k-1} \cdot e^{-(\frac{U}{a})^k} \tag{55}$$

Here k is the shape parameter, a is the scale parameter and U is the wind speed.

The Weibull distribution was used to determine the probability of bins with a width of 0.5 m/s. An example of these bins can be seen in figure 13.

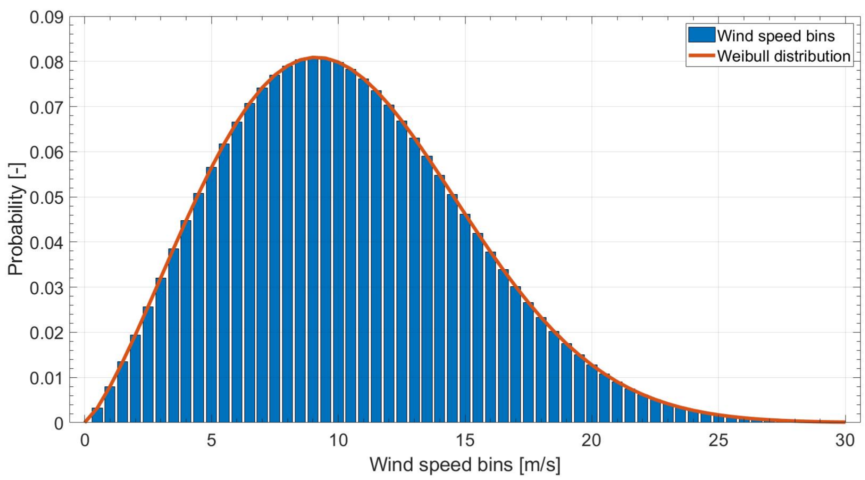

Figure 13: Wind speed bins and Weibull distribution with a = 11.7 and k = 2.3

These probabilities of each wind speed occurring were combined with the production curve to determine how often each amount of hydrogen production level is achieved during a year. By multiplying this with the 8760 hours in a year, the yearly production per turbine without any availability or other losses for that specific power rating is calculated.

The efficiency of electrolysers is assumed to drop yearly by 0.5%. Therefore, the annual production of hydrogen for each specific year of the design life of the turbine is calculated using equation 56.

$$AHP(t) = AHP(1) \cdot (1-\gamma)^(t-1) \tag{56}$$

Here, $AHP(t)$ is the hydrogen production in kilograms in year t, $AHP(1)$ is the hydrogen production in the first year, where no efficiency losses of the electrolyser occur and γ is the efficiency loss. Through this method, the total amount of hydrogen produced for each relevant power rating is determined.

3.4.2 Farm losses

In order to create a more realistic final result, three losses were taken into account; wake losses, the availability of the wind farm and the availability of the pipeline infrastructure. For each loss, a percentage is assumed. The wind farm availability states what percentage of the total possible production at the farm, according to the available wind, is actually produced. The availability of the pipeline infrastructure describes what percentage of the total operation hours, the pipeline is not malfunctioning or has any other defect, resulting in a loss of production. The wind farm and pipeline availability have an expected value of 95% and 99.7%. The wind farm availability of 95% is based on data by SPARTA on the availability of offshore wind farms in the UK [34]. SPARTA is a British platform for data sharing on offshore wind farms. The pipeline availability is based on information from Gasunie, the owner of the Dutch natural gas infrastructure. They experienced an availability of "almost 100%" in 2019, which has been translated to 99.7% in this model [35]. It should be noted that this availability is based on onshore natural gas transport. Offshore might have a lower availability, but 99.7% is considered reasonable in this model.

Wake losses are a third loss mechanism that is of great importance for the reliability of the case study. During the design of a wind farm, the wake losses are normally as completely computed as possible. The exact amount of wake losses due to an increased power capacity requires extensive wind farm design and wake analysis. However, this model only uses a simple approach to the losses resulting from wake, without any extensive wind farm design.

Furthermore, wake losses are normally at least partially compensated by increasing the distance between the turbines. This itself creates new problems, since a larger distance between the turbines will require more pipelines, which will result in a different LCoH. Also, a larger distance between the turbines also means that the area required for the wind farm increases, which creates a social issue with how much space is available, which is outside the scope of this thesis. Therefore, the distance between the turbines at different power capacities is assumed constant in this model.

Wake is the decrease of energy available in the wind due to both a decrease of wind speed and turbulent air behind a wind turbine. This lower wind speed at the next turbine will result in a shift to the left on the power curve, lowering the amount of hydrogen produced. As can be seen in figure 15, the biggest drop in power occurs near rated wind speed, since the power curve is steepest in that area. The wind speed resulting from a wake is described by equation 57:

$$1 - \frac{U_w}{U} = \frac{1-\sqrt{1-C_T}}{(1+2ks)^2} \tag{57}$$

where U_w is the lowered wind speed due to wake, U is the undisturbed wind speed, C_T is the thrust coefficient, k is the wake decay coefficient and s is a dimensionless distance behind the turbine at which the lowered wind speed occurs. As can be seen in equation 57, if C_T approaches zero, the term on the right (and therefore also the left) will approach zero. The term on the left approaches zero when the lowered wind speed will approach the undisturbed wind speed. Therefore, a lower C_T will result in a higher U_w.

When the power rating of the turbine is increased, the power curve remains the same below the old rated wind speed, as can be seen in figure 15. Therefore, the wake losses at low wind speeds will remain constant, independent of an increase in power capacity. At wind speeds far above the rated wind speed, the thrust coefficient drops to near zero, as can be seen in the Thrust Coefficient - Wind speed curve in figure 14. Due to this low thrust coefficient, at high wind speeds, the U_w as described above will be closer to the undisturbed wind speed, eliminating the wake loss effects.

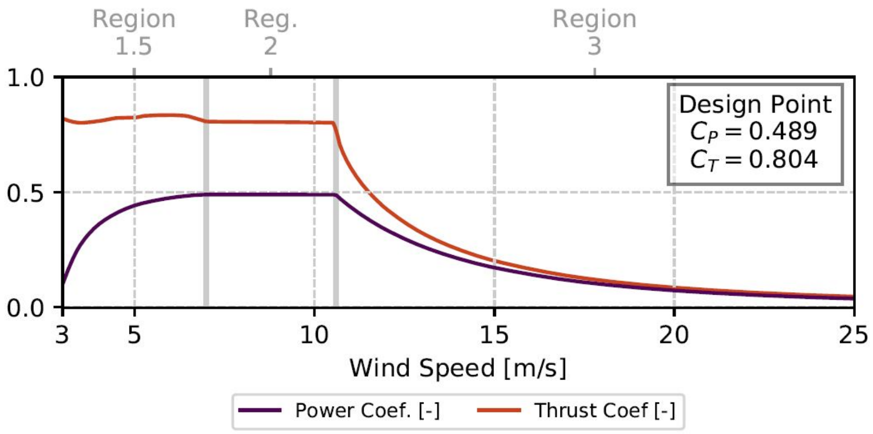

Figure 14: The power and thrust coefficient plotted against wind speed for a 15 MW reference turbine [8]

Around rated wind speed and above, the power curve continues on the same path as before the original rated wind speed, which can also be seen in figure 15. This results in a larger amount of wind speeds were a small change in speed results in a large change in power produced. Therefore, one expects that a wind farm containing turbines with a higher power rating would have much higher losses due to wake. However, some of the effects described above are compensated due to available wind. As can be seen in the Weibull curve in figure 13, the higher rated wind speeds of higher power capacity turbines occur less and less often the higher one goes. Therefore, the drop in wind speed due to a wake results in larger losses for higher power capacity turbines. However, since the chance that this drop in wind speed occurs is lower, it is limited how much higher the wake losses will be due to an increase in power capacity.

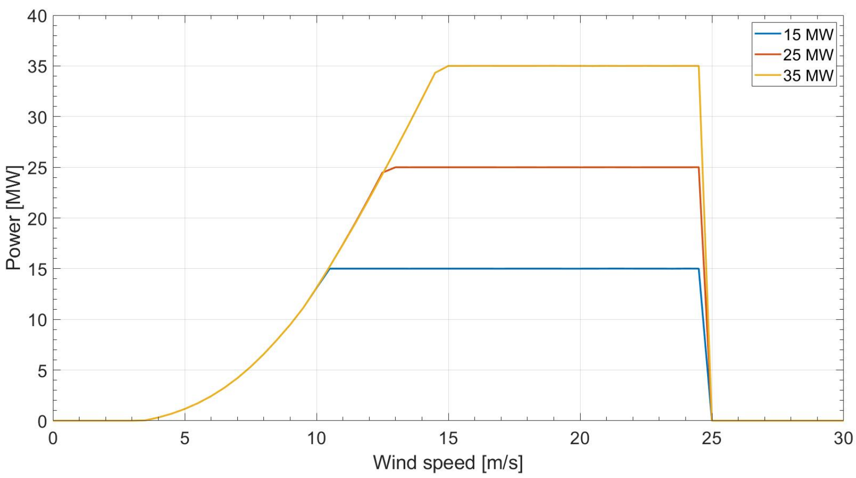

Figure 15: Power curves for 15, 25 and 35 [MW] wind turbines

This model assumes a simpler approach to the wake losses, due to the reasons stated above. Here, the wake losses are an average for the entire wind farm. Furthermore, a linear correlation between the power capacity of the turbines and the wake losses is assumed. This approach is lacking in exactness, but is still included, since a simple approach is better than no approach. Also, modelling the wake allows the possibility of assessing the sensitivity of the wake values, giving information on the importance of wake modelling. The wake losses of the reference wind farm of around 1 GW is set at 10%. The wake loss increases with 0.4% for each MW added to the power capacity of the turbines on the farm. Both the base wake loss and the increase per megawatt are based on a confidential study by Vestas, where similar wake loss ranges are found. Below, equation 58 gives the function used to calculate the wake loss.

$$\mathrm{WL}_{new} = 0.10 + (4 \cdot 10^{-6} + \mathrm{WF}) \cdot (P_{new} - P_{ref}) \tag{58}$$

Here, WL is the wake losses, WF is a factor to vary steepness of wake loss increase, while P is the power rating in kW.

4 Results

This section states the results from the previously described model. First, a case study used to obtain results for a specific scenario is described. The results from this case study are presented, as well as a deeper review of the case study results.

4.1 System specifications for the case study

4.1.1 Turbine specifications for the case study

The hydrogen turbines designed in this case study are based on the IEA 15 MW reference turbine [8]. This turbine has a rotor diameter of 240 meters, meaning the original specific power is equal to 332 W/m^2 This turbine was chosen as the base point, since IEA Wind TCP Task 37 provides a complete and thorough description of the turbine. Furthermore, IEA Wind TCP Task 37 has created several other reference turbines, which have been used in research before. The 15 MW reference turbine information has been released in 2020, therefore making it up-to-date at the time of writing this thesis. 15 MW turbines are the size the industry is currently moving towards, as can be seen by the SG 14-222 DD 14 MW turbine produced by Siemens Gamesa [36]. Some other relevant information for this turbine can be found in table 6, including rated wind speed. Other information on the IEA 15 MW reference turbine can be found in the technical report where the definition of the turbine is given [8].

The design life of both the hydrogen turbines and the electrolysers is set at 20 years, therefore setting the wind farm design life at the same age. The industry standard for wind turbine design life is 20 years and the design life of the PEM stacks is also set at 20 years based on information from HYGRO supplier PlugPower.

As a standard, the inflation is assumed to be 2.2% and the interest rate 4%, based on a European Commission report for large scale energy projects with a lifetime of 25 years [37]. Combining these in equation 3, a discount rate of 1.76% is found.

4.1.2 Wind farm specifications for the case study

The reference size of the wind farm is set at 1,005 MW. This wind farm is made up of 67 turbines with a power capacity of 15 MW. The location chosen for the wind farm in this case study is at FINO1 [38], which is a research platform in the North Sea, north of the province of Groningen. The location has a depth of 30 meters. This location was chosen, since within the Netherlands, the province of Groningen is aiming to become the production hub of hydrogen. The on-land location that is most relevant for this is Eemshaven, near the German border. The distance from FINO1 to this onshore location is 60 kilometers. Figure 16 shows the exact location of FINO1. Weibull data is available for FINO1 through the Dutch institute KNMI for the period 2004-2013 [39]. Since the Weibull parameters are dependent on height, the hub height of 150 meters was chosen as the reference point. The scale parameter at this height is 11.7 and the shape parameter 2.3. The average wind speed at a height of 150 meters is 10.36 m/s.

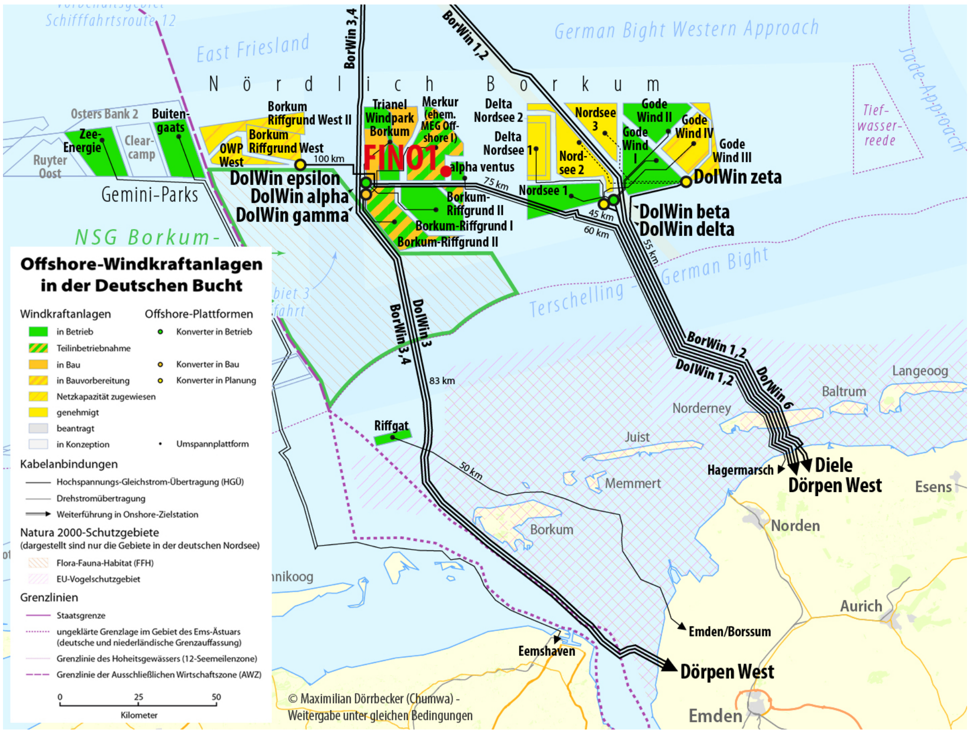

Figure 16: Location of FINO1 [38]

4.1.3 Production specifications for the case study

As described in section 3.4.1, in order to determine the production level for each power capacity, power curves for these power capacities are needed. Using the program FASTTool [40], power curves for turbines with rated power of 15 up to 35 MW were made. Since creating a hydrogen production curve for each power capacity was not possible for HYGRO, production curves in steps of 2.5 MW were made. 2.5 MW was chosen as a step size since this is the maximum size of the electrolyser stacks, as described in section 2.2.1. The hydrogen production power curve of the reference 15 MW turbine can be seen in figure 12. In order to determine the production levels in between the 2.5 MW steps, a two term power series fit is used. This fit was used on the nine discounted, total hydrogen production values resulting from the power curves, similar to the sum in the denominator in equation 1 in chapter 3. The resulting discounted production amounts can be seen in figure 17 plotted against different power capacities.

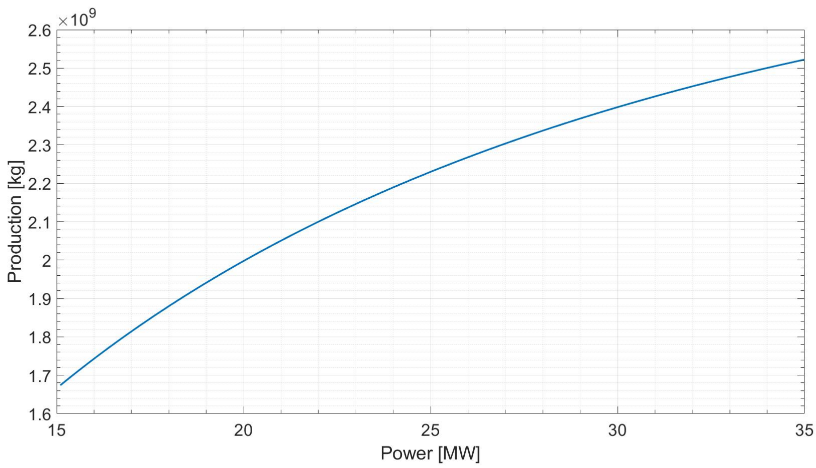

Figure 17: Discounted total hydrogen production for different power capacities

Table 6: Summary of IEA 15 MW reference turbine

Rated power	15 [MW]
Turbine class	IEC class 1B
Power density	332 [W/m^2]
Number of blades	3 [-]
Cut-in wind speed	3 [m/s]
Rated wind speed	10.59 [m/s]
Cut-out wind speed	25 [m/s]
Rotor diameter	240 [m]
Hub height	150 [m]
Drivetrain	Low speed direct drive
Design λ	9 [-]
Min. rotor speed	5 [rpm]
Max. rotor speed	7.56 [rpm]
Max. tip speed	95 [m/s]
Blade mass	65 [t]
Tower mass	860 [t]
Tower base diameter	10 [m]
Tower top diameter	6.5 [m]
Transition piece height	15 [m]
Monopile embedment depth	45 [m]
Monopile mass	1,318 [t]
Designed sea depth	30 [m]
Design C_P	0.489 [-]
Yaw system mass	100 [t]
Pitch system mass	8 [t]
Bearings	7.9 [t]
Shaft	15.7 [t]
Miscellaneous components mass	65.3 [t]

4.1.4 Model variables for the case study

The model includes several variables that need to be set before running. An overview of the values of these components is given in table 7. The reasoning for choosing these values is given below.

Table 7: Overview of values of variables for modelling during case study

Variable	**Value**
Generator scaling variable Ξ	1.06
Blade mass variable X	0.84
Blade cost per kilogram P_b [€/kg]	14.60
Tower mass variable $f_{u,\ T}$	1
Transition piece mass variable $f_{u,\ TP}$	1
Monopile mass variable $f_{u,\ M}$	1
Monopile embedment depth variable χ	3
Wake variable WF	0.00

The generator scaling variable Ξ is used to increase the scaling of the cost of the generator at higher power capacities, as explained in section 3.3.4. In this case study, the variable has a value of 1.06. This value was chosen, since compared to a situation where the variable is set to 1, the cost will increase by 5% when scaled up from 15 to 35 MW.

The blades have two variables. The first variable decreases the thickness factor, therefore decreasing the blade mass after scaling. It is set at 0.84, since this would yield a decrease of blade mass of 5% when scaled up to 35 MW compared to a situation where the variable is set to 1, similar to the generator scaling variable. The blade cost is the second variable. It is set at 14.6 €/kg as described in the section 3.3.6, since that is the average cost per unit mass in the report by BVG [20].

The tower variable $f_{u,\ T}$, transition piece variable $f_{u,\ TP}$ and monopile variable $f_{u,\ M}$ all describe the accuracy of the determined volume. When set at 1, as done in this case study, the determined dimensions are not corrected.

The monopile embedment depth variable χ is set at 3, since this would result in the overtuning moment dominating the design, as stated it would in section 3.3.11.

The value of the wake factor variable WF is set at zero in the case study. This was done in order to have the wake loss increase by 0.4% per MW added to the power capacity, which is closest to the data in the confidential study by Vestas.

4.2 Case study results

Figure 18 shows the LCoH for different power capacities as a result of scaling from the 15 MW reference turbine. The minimum value of the LCoH is at 27.6 MW, with a value of 1.6938 €/kg H_2. A breakdown of the 27.6 MW turbine can be seen in table 8. Here, the third column described the percentage increase compared to the reference turbine.

Table 8: Summary of the 27.6 MW up-scaled turbine

Rated power	27.6 [MW]	+84 [%]
Power density	610 [W/m^2]	+84 [%]
Rated wind speed	13.36 [m/s]	+26 [%]
λ at rated wind speed	7.11 [-]	-21 [%]
Blade mass	79.5 [t]	+22 [%]
Tower mass	976 [t]	+13 [%]
Tower base diameter	10.81 [m]	+8 [%]
Monopile embedment depth	47.41 [m]	+5 [%]
Monopile mass	1,593 [t]	+21 [%]
Transition piece mass	117 [t]	+17 [%]
Rated C_P	0.450 [-]	-8 [%]
Blade thickness factor	1.265 [-]	+26.5 [%]
Wake losses	15.04 [%]	5.04 [p.p.]
Production amount	2,324 $\cdot 10^6$ [t H_2]	+39 [%]
Hub mass	278 [t]	+46 [%]
Bedplate mass	105 [t]	+50 [%]
Generator mass	743 [t]	+63 [%]
Converter mass	26.7 [t]	+78 [%]

Several things can be noted from table 8. Firstly, most component masses do not increase as much as the power. Furthermore, the value of the thickness factor appears reasonable. Lastly, both the C_p and λ have been lowered, but the decrease is not extreme.

An important point on the resulting turbine is the possible problems in manufacturing. Since some components are scaled up to a size currently not produced, there might be issues in production. Blades at a size of that of the 27.6 MW turbine are so large, that current production methods might not be able to stand up to the task of production. The same can be said for the generator size, which currently doesn't exist for a 27.6 MW turbine. Other solutions for the generator might be necessary at these power capacities for the generator to be put in production.

A wind farm with 67 of these 27.6 MW turbines would result in a total wind farm rated power of 1,849.2 MW. The total turbine cost is equal to €27,729,000 and the total wind farm costs are equal to €3,936,300,000.

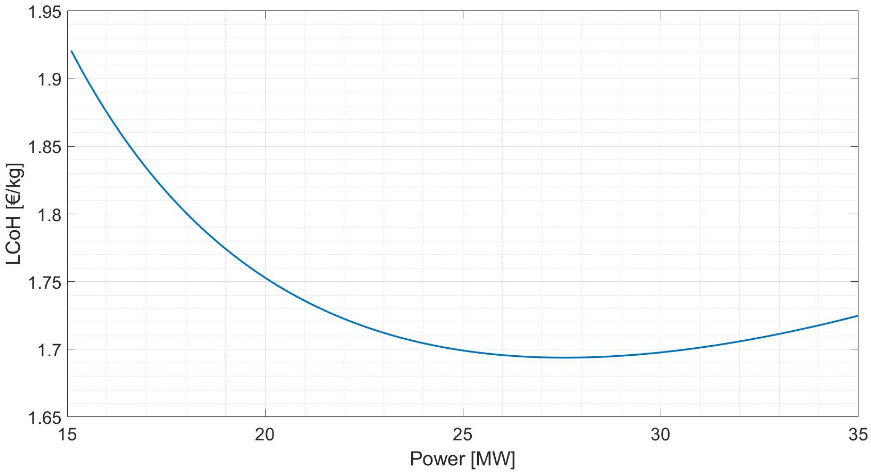

Figure 18: Resulting LCoH for different power capacities in the case study

As can be seen in figure 18, the LCoH drops rapidly at first, then leveling out around 25 MW and going up again around 30 MW. This means that the optimal level of 27.6 MW might be the minimum point of the graph, but the difference in LCoH between 25 MW, 27.6 MW and 30 MW is limited. Therefore, it is better to say that the optimum lays somewhere in the range between 25 and 30 MW.

Another noticeable result is that the LCoH of the 15 MW reference turbine is already lower than the current green hydrogen LCoH (1.93 vs. 2.50 €/kg). This suggests that even a normal 15 MW wind turbine converted to a hydrogen turbine would already be more price competitive than current green hydrogen production methods. It is however still around 30% more expensive than grey hydrogen at 1.50 €/kg. The lowest LCoH achieved at 1.6938 €/kg is still higher than the grey hydrogen value, but does approach it and is around 13% higher.

The fact that the LCoH curve has a minimum suggests that after a certain point, the increase in production level is no longer high enough to cover the extra costs of the larger turbine. In order to validate this, the cost of the components of the turbine and the farm are relevant. These costs can be seen for a 15, 25, 27.6, 30 and 35 MW turbine in figure 19 and 20. What is most noticeable in figure 19, is that the costs of the electrolyser and generator are highest, as well as most rapidly increasing with higher power capacities. Looking at figure 20, the turbine is also the biggest contributor to the total cost of the farm. Therefore, the electrolyser and generator are both the most important components for defining the final cost and have the most effect on the numerator of the LCoH as seen in equation 1. Both the electrolyser and generator are the most expensive components of a hydrogen turbine. Furthermore, both scale linearly with the power capacity, making their cost increase quicker than other components.

Figure 17 depicts the total, discounted production levels for different power capacities. As can be seen, the curve flattens at higher power capacities. The flattening will also have an effect on the increase in LCoH curve as seen in figure 18, since a flatter curve results in fewer extra units produced for an extra unit of power capacity. There are several explanations for this. Firstly, the production needs to be discounted to be used in the calculation of the LCoH as seen in equation 1. Secondly, the efficiency of the electrolyser stacks is assumed to drop by 0.5% every year. Both of these things mean that in the last year of production, the amount is decreased by a percentage. Since it is a percentage and not a constant value, at higher possible production levels, the amount of production decrease will also be higher.

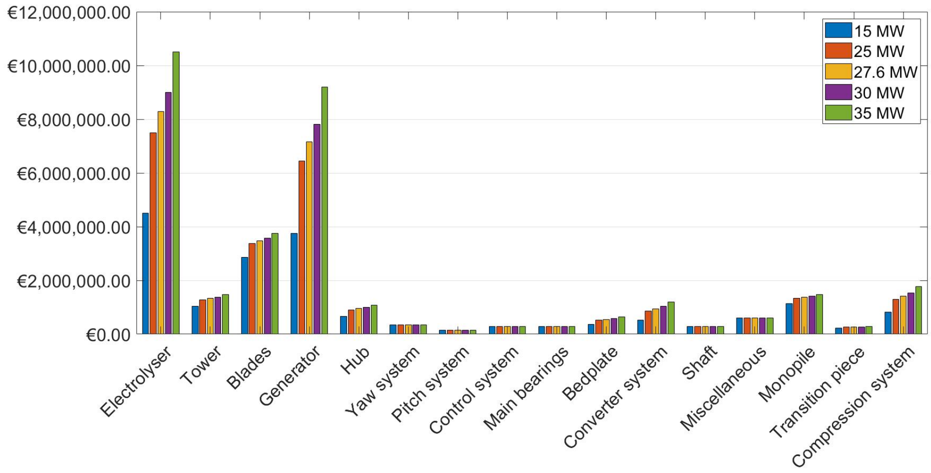

Figure 19: Cost for different components of a 15, 20, 27.6, 30 and 35 MW turbine

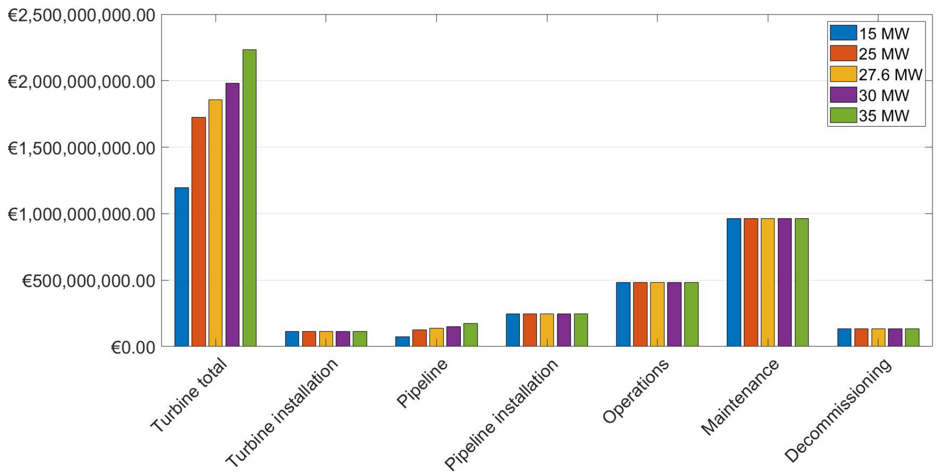

Figure 20: Cost for different farm configurations with 15, 25, 27.6, 30 or 35 MW turbines

Another reason for the flattening out is that hydrogen turbines with higher power capacities will also have a higher rated wind speed. Since the chance that a wind speed occurs lowers at higher wind speeds, the chance of the hydrogen turbine running at its rated power is also less likely. Therefore, the hydrogen turbine could potentially produce more, but the wind conditions do not allow for that.

A last reason for the flattening out of the production curve is the increasing amount of wake losses at higher power capacities. Since each turbine will take more energy out of the wind at higher power capacities, the amount of energy left for the turbine behind it will be lower. Since the model uses a simple wake model, this decrease in production due to wake losses is only connected to the power capacity of the turbines.

4.3 Results review

In this section, several different methods are used to review the case study results, as well as the model. First, variations in the scaling variables are discussed. Next, the effects of variations in the used discount rate are investigated, followed lastly by an investigation into the effects of variations in the average wind speed.

4.3.1 Variations in scaling variables

In order to review the case study results, an error analysis is performed. There are several components in the model that can have a varied input. These seven variables can be seen in table 9. To determine the effects of changing these variables, 10,000 runs were performed. During each run, the LCoH is calculated for a power rating ranging from 15 MW up to 35 MW in steps of 0.1 MW. For each run, every variable was assigned a random value between the given variation, so each of the 10,000 runs results in a different outcome. In order to validate the ranges of the variables, eight other variations were performed. Here, in each variation, all but one variable were kept constant. The other variable set to a random value in the same range as seen in table 9. This allowed insight in the effects of the variable on the results.

Table 9: Overview of variation of variables for modelling during case study

Variable	**Value**
Generator scaling variable Ξ	1.00 - 1.11
Blade mass variable X	0.67 - 1.00
Blade cost per kilogram P_b [€/kg]	12.50 - 16.70
Tower mass variable $f_{u,\ T}$	0.80 - 1.20
Transition piece mass variable $f_{u,\ TP}$	0.70 - 1.30
Monopile mass variable $f_{u,\ M}$	0.70 - 1.30
Monopile embedment depth variable χ	2.980 - 3.005
Wake variable WF	-2 $\cdot 10^{-6} - 2 \cdot 10^{-9}$

Firstly, the scaling variable for the generator Ξ is set between 1 and 1.11. The reasoning behind this is that at much higher power ratings than the reference, the generator cost is not likely to still scale linearly with power. Therefore, an increase of cost by 10% at a 133% power capacity increase was chosen as the upper cost limit. To achieve this 10% increase, the variable has to be set at 1.11. Because of this, the variable was set to have a random value between 1 and 1.11.

The blade model has two variables, the decrease of the blade mass (X) and the cost of the blades (P_b). The blade mass variable ranges from 0.67 up to 1. The lower value was chosen as such, since it would result in a decrease of mass of 10% when power capacity is increased by 133%. This is assumed to be a reasonable decrease in blade mass in the extremest case. The cost of the blades were varied between 12.50 and 16.70 €/kg, since that is the range in which the report by BVG Associates assumes the blade cost to be [20] as stated before in section 3.3.6.

The variables $f_{u,\ T}$, $f_{u,\ TP}$ and $f_{u,\ M}$ were chosen to depict a range within which the dimensions of the tower, transition piece and top of the monopile were expected to lay. The ranges as given in table 9 are set as such, since this allows the volume of the tower to vary 5% in both directions. An actual designed tower, transition piece or top of the monopile is expected to have a mass, thus volume, within that range.

The monopile variable χ ranges from 0.2980 up to 3.005. The lower bound was set so that the depths found would be near the results for a situation as described in [32], where the moment is equal to zero, as seen in equation 52. This is seen as the extreme case for the monopile depth. The upper bound of 3.005 is set to lower the monopile depth slightly, since it is not a precise model and it does not take into account variations of the soil at great depths.

The wake loss factor was set randomly between $-2 \cdot 10^{-6}$ and $2 \cdot 10^{-6}$ in order to get a wake loss between 14 and 22 % at the maximum power rating of 35 MW, This range is assumed to be a reasonable approach for wake losses at a wind farm of this size, since it is a wide range and the wake loss modelling is imperfect, so a large range allows insight in the effects.

4.3.2 Results from variation in scaling variables

The LCoH boxplot resulting from variation in the scaling variables can be seen in figure 21. It depicts the variation in LCoH for several chosen power capacities. Here, the red line is the median value and the blue box around it depict the 25th and 75th percentile. The outer lines for each power capacity are the most extreme outliers for that data point.

The median LCoH lowers rapidly with an increasing power capacity until around 25 MW, after which it levels out and eventually starts rising again around 30 MW. The LCoH in the range where the curve is flattened out is around 1.69 €/kg. This is a decrease of 12.2% from the 15 MW reference turbine's median LCoH of 1.925 €/kg. Furthermore, with an increasing power capacity, the uncertainty of the LCoH results become bigger, making it harder to pinpoint an exact value for the LCoH. At 27.5 MW, the difference between the 25th and 75th percentile is 0.05 €/kg, while at 35 MW this difference is 0.10 €/kg.

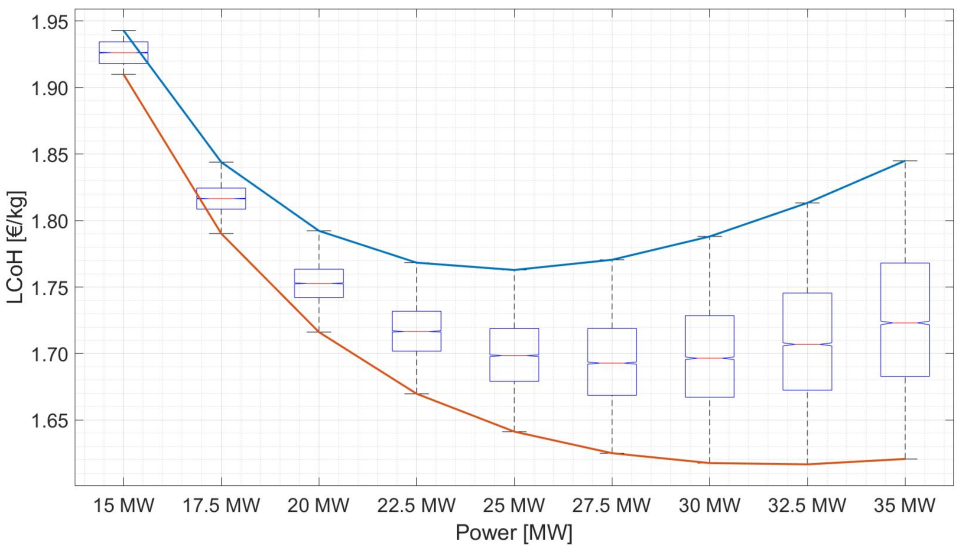

Figure 21: Boxplot of LCoH variation of different power capacities when the scaling variables are randomised

The optimal power capacity is determined by finding the point at which the LCoH is lowest for each run. The probability of each power capacity being optimal in the 10,000 runs as described above can be seen in figure 22. Here it can be seen that the optimal power capacity clearly is somewhere between 25 MW and 31.5 MW. This range is comparable to the range in which the LCoH has flattened out in figure 21. Furthermore, it can be seen that the probability of the optimal power being between 25 and 28 MW is higher than the probability of it being between 28 and 31.5 MW, which means that the optimal power is more likely to be in the lower range (25 to 28 MW).

A probable reason for this can be found by looking at the uncertainty as depicted in the boxplot of the LCoH in figure 21. As stated before, the LCoH at lower power capacities has a much higher certainty. When looking at the points for 25 MW and 27.5 MW, it can be seen that both have a similar median value. However, the range within which the results lay is smaller at 25 MW. This is depicted by the two lines going through the extreme cases in figure 21. The extreme value are a result of variables having similar values. As can be seen, the highest possible case at 25 MW is lower than at 27.5 MW. However, the median is similar for both. Therefore, the possible LCoH curves are likely to follow a curve somewhere between the upper bounds and median. In that case, the minimal LCoH is more likely to be around 25 MW rather than 27.5 MW. In the lowest possible case, the LCoH of 27.5 is lower than that of 25 MW. However, the LCoH at 30

MW is even lower. Therefore, in the cases below the median, the lowest LCoH is likely to be somewhere between 27.5 and 32.5 MW, which suggest a wider spread of optimal results. This can be seen in figure 22, where the values between 25 MW and 28 MW are more likely, while above 28 MW, there is a wider spread of possible optimal power capacities at lower probabilities.

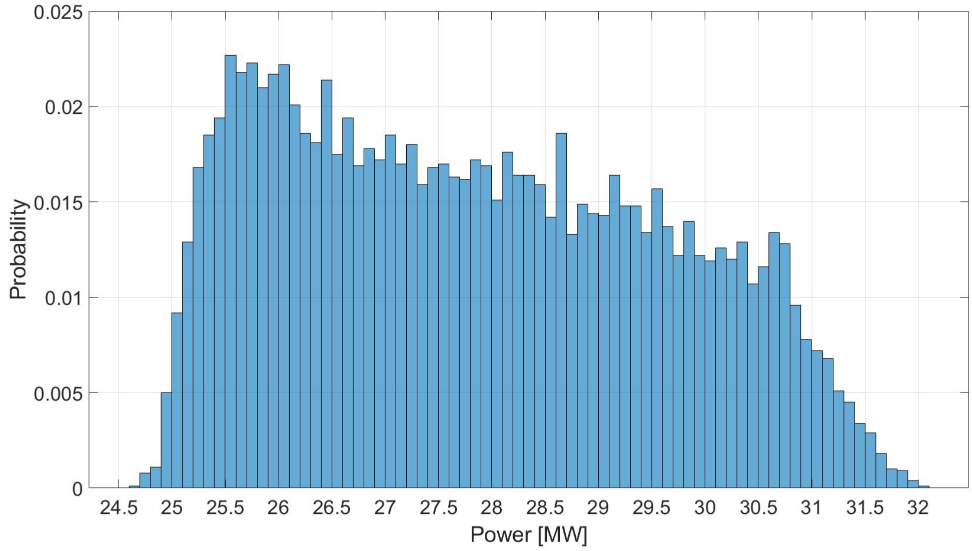

Figure 22: Probability histogram of optimal power capacities when the scaling variables are randomised

Since there is a range of possible optimal power capacities, figure 23 and 24 depict the cost for all components and the wind farm for three different power capacities. Error bars are also included in these figures, but these error bars are small, therefore suggesting the cost results have a higher certainty. The error bars depict the 25th and 75th percentile. Table 10 gives the minimum and maximum cost of 15, 25 and 30 MW turbine and wind farm.

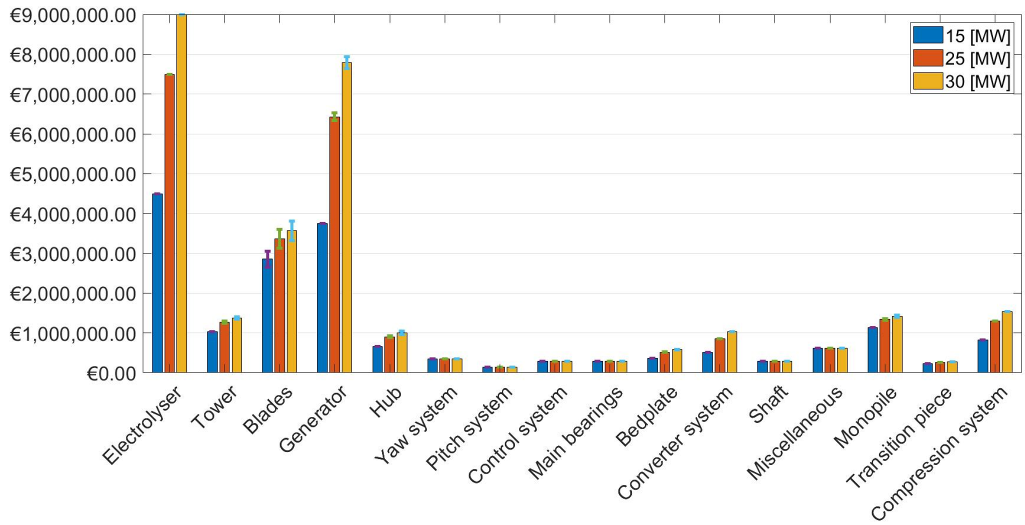

Figure 23: Cost of components of a 15, 25 and 30 MW turbine

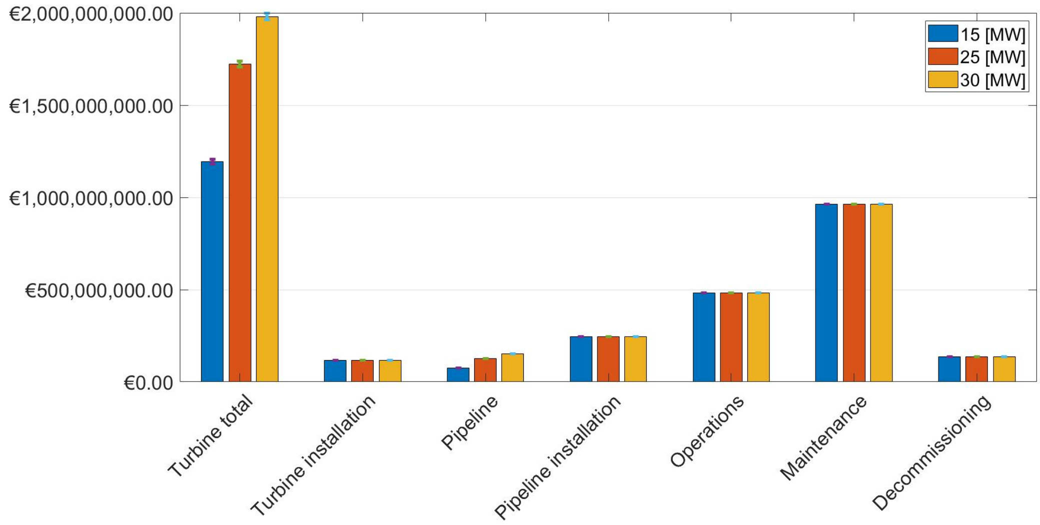

Figure 24: Cost for different farm configurations with 15, 25 or 30 MW turbines

Table 10: Cost of turbine and wind farm for several power capacities

Power	15 MW	25 MW	30 MW
Turbine	€17,414,000 - €18,236,000	€24,850,000 - €26,568,000	€28,465,000 - €30,653,000
Farm	€3,181,900,000 - €3,237,000,000	€3,730,300,000 - €3,845,500,000	€3,997,700,000 - €4,144,300,000

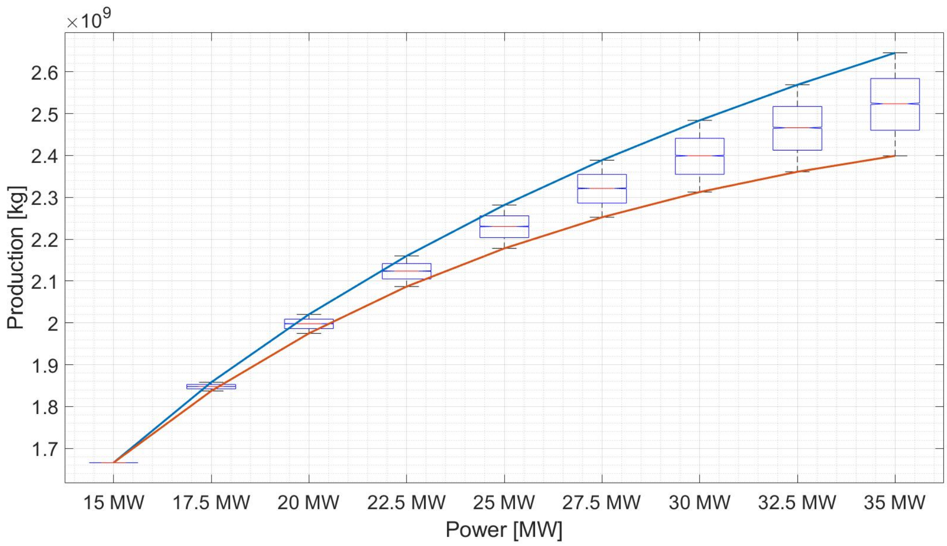

Figure 25: Boxplot of discounted production amounts

Because the variation in cost is minimal, the variation in LCoH will have to be a result of the production. Figure 25 shows the discounted production for different power capacities in a boxplot. As can be seen, the variation in production increases at higher power capacities. The maximum production at 35 MW is 10% higher than the minimum production at 35 MW, which is a difference of 240,000,000 kg. The variation in production can only be a result of the wake factor WF, since that is the only variable that affects the production.

As stated before, the importance of each variable on the results have also been investigated. Below, figure 26 shows the spread of the optimal power capacity when all of the variables are kept constant, except for the one given on the x-axis, which is randomised according to the ranges given in table 9. For comparison, the spread in case of all variables being randomised is given as well. As can be seen, the median optimal power capacity constantly lays somewhere between 27 and 28 MW. Also, the first seven variables clearly have a more limited effect on the spread of optimal power capacity. However, a randomised wake factor WF does drastically affect the spreading of the result. This suggests again that the wake factor has the most effect on the optimal result, since keeping it constant hardly results in variation in the results. The wake factor does not affect the cost of the turbines, only the amount of production, which is used in the denominator of the LCoH equation (equation 1).

Figure 27 contains the boxplots of the LCoH for the median optimal power capacity of each variable. For this figure, first, the optimal power for each of the 10,000 runs was determined. Next, the median of all these optimal powers was calculated. At that optimal power, the spread in LCoH is given in figure 27. Similar as for the power capacity described above, the median LCoH value remains relatively constant, around 1.69 €/kg. Furthermore, the effect of the wake factor is again clearly visible in the larger spread in results. This larger spread was noted before as well, while looking at the spread of the production in figure 25. From this can be concluded that in the model, the wake factor has the largest effect on the final results.

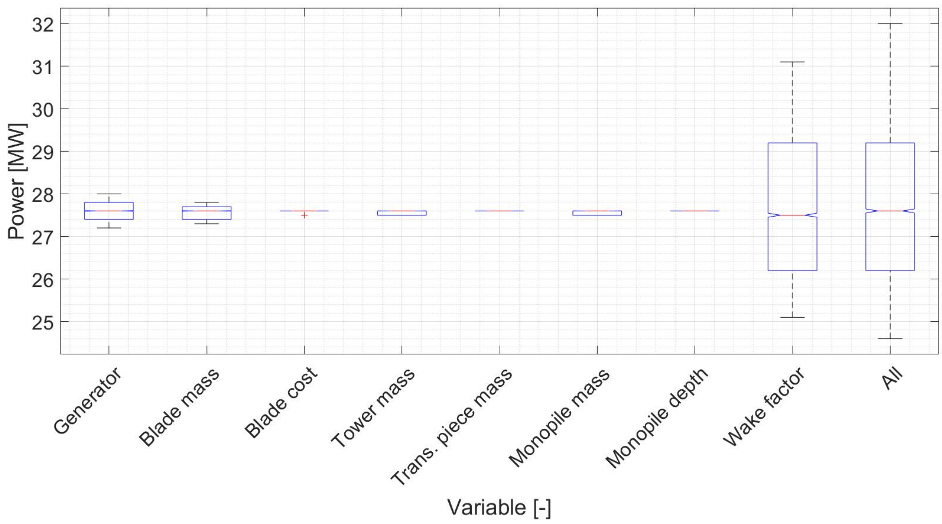

Figure 26: Boxplot of optimal power variation with different randomised variables

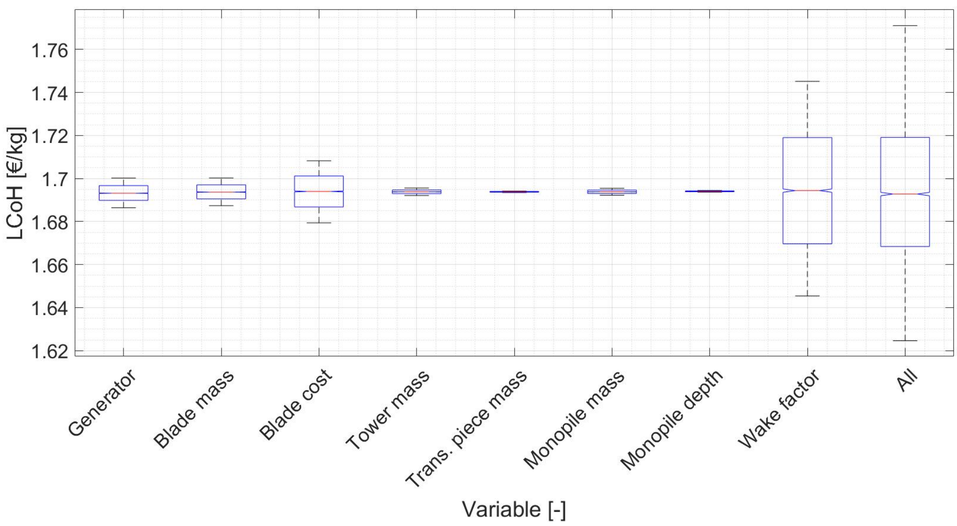

Figure 27: Boxplot of LCoH variation for different randomised variables at their optimal power

4.3.3 Variation in discount rate

Due to the unpredictability of the economy, the inflation and interest rate should also vary from their original value of 2.2% and 4%. Since both are combined in the discount rate d, only that variable needs to be changed to see the effects of different economic situations. Therefore, the discount rate was varied from 0.25% up to 5.0% in steps of 0.25%. For all twenty values of the discount rate, 10,000 runs were performed, where in each run, the LCoH for a power capacity between 15 and 35 MW was calculated. These runs maintained the same random variations as described before in section 4.3.1. All other conditions were kept the same from the variations in scaling variables results in section 4.3.1.

The summarised results are given in figure 28 and 29. As can be seen, a higher discount rate results in a downward shift in the optimal power capacity and an upwards shift in LCoH at the median optimal power capacity. However, the downward shift is not rapid and even in an unrealistic scenario where the discount rate is equal to 5%, the optimal power will still always be above 23 MW and likely be above 25 MW. Furthermore, in the case of an extremely low discount rate of 0.25 %, the optimal power capacity in the extremest case can reach a level of just below 34 MW.

Figure 29 shows what the LCoH of the median optimal power capacity would be. The median LCoH increases at higher discount rates, ranging from 1.68 €/kg at a discount rate of 0.25% up to 1.95 €/kg at a rate of 5%. At the lowest discount rate, the LCoH approaches the cost of grey hydrogen in Europe, but never reaches it. The upward shift at higher discount rate can be explained through equation 1. Here, if the cost and amount produced each year remain the same, future cost and production will have less importance on the LCoH at a high discount rate, since the costs mainly are CAPEX. A high discount rate is a result of either a high interest rate or low inflation or a combination of both. A high interest rate results in future costs becoming higher, so debts resulting from CAPEX become more expensive. A low inflation rate suggests that future earned money is less valuable. Therefore, product sold in the future is less valuable. A high discount rate would push the entire LCoH curve up along the y-axis, since the total CAPEX costs become higher. This is clearly visible in figure 29 in the upwards trend of the LCoH at higher discount rates.

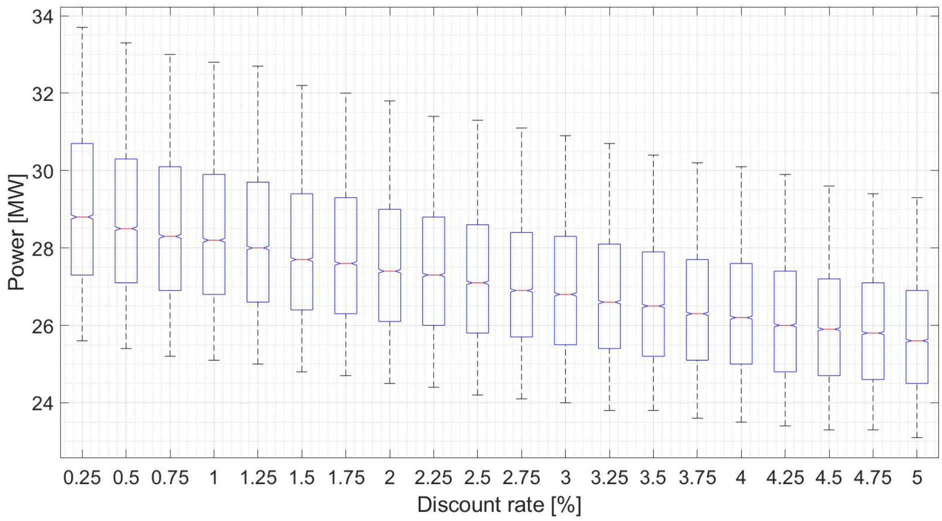

Figure 28: Boxplot of optimal power variation of different discount rates

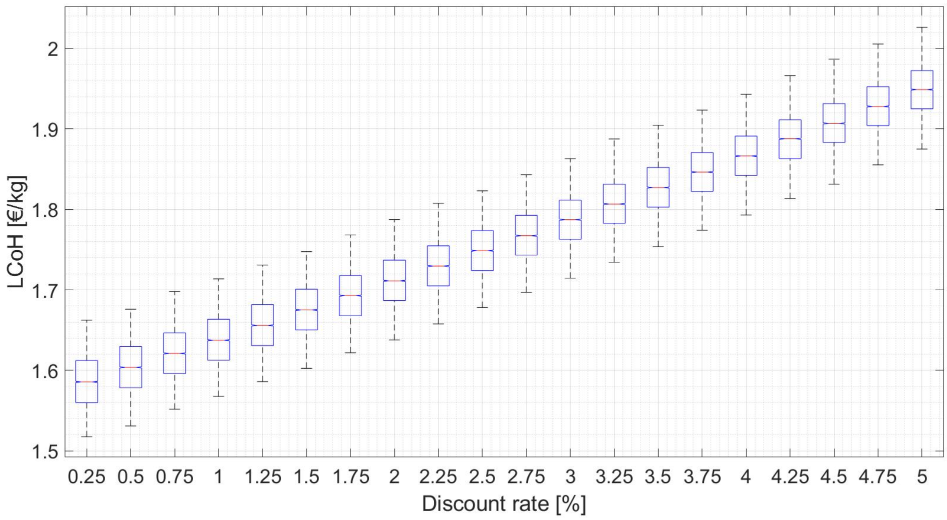

Figure 29: Boxplot of LCoH variation of different discount rates at the median optimal rated power

In order to take a closer look at the two extreme cases, the LCoH boxplot for a discount rate of 0.25% and 5% are given below in figure 30 and 31. The area around the optimal power as given in figure 28 is of the most importance. In the case of a discount rate of 0.25%, the LCoH curve mostly has flattened out after 25 MW and only slightly starts rising again after 32.5 MW. This suggests that the median optimal power might be around 29 MW, the difference in median LCoH between 25 MW and 32.5 is just 0.01 €/kg. Something similar is visible in the case of a discount rate of 5%. Here, the median of the optimal power is at around 25 MW. However, the LCoH has flattened out in the range of 22.5 MW up to slightly below 30 MW, where the median variation is again 0.01 €/kg.

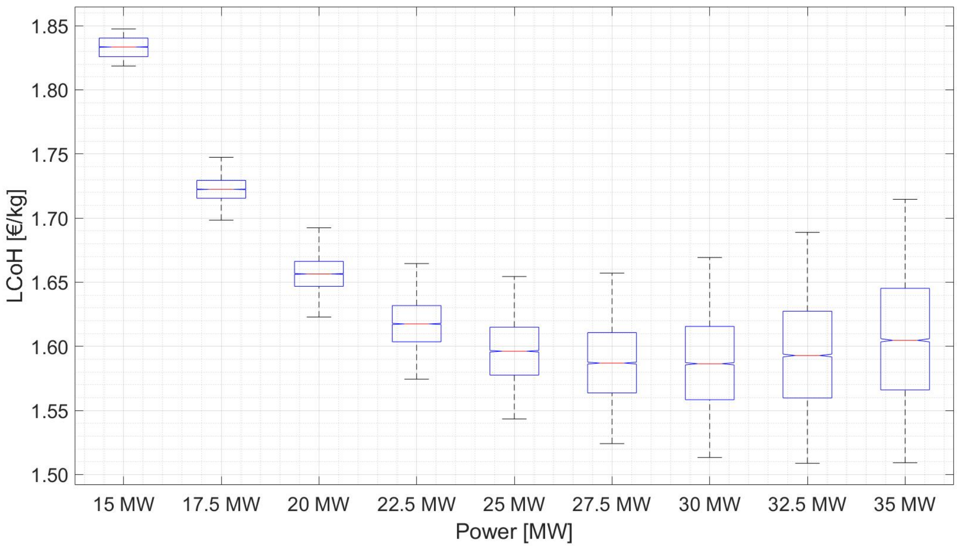

Figure 30: Boxplot of LCoH variation of different power capacities at a discount rate of 0.25%

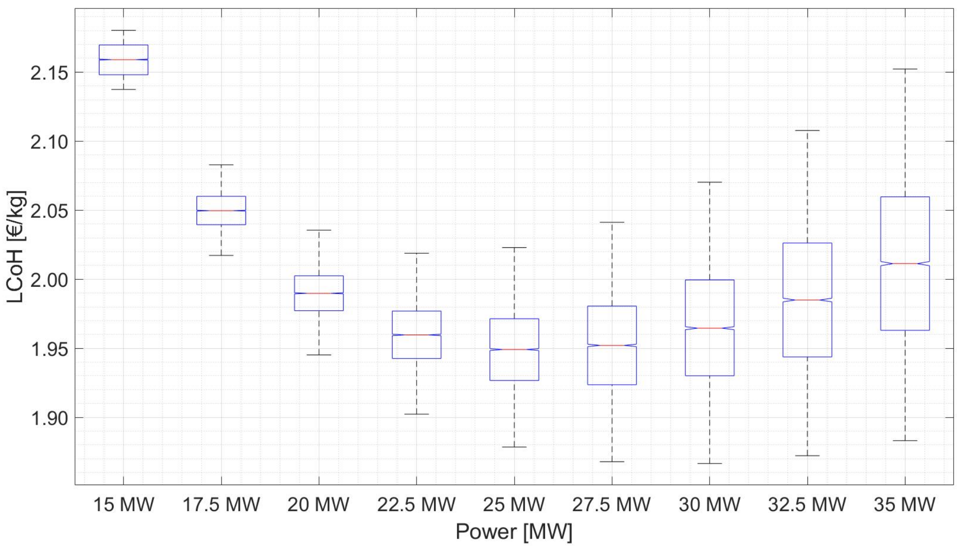

Figure 31: Boxplot of LCoH variation of different power capacities at a discount rate of 5%

4.3.4 Variation in average wind speed

Lastly, in order to see how the model performs under different wind conditions, the average wind speed was varied. All other variables were set in a similar randomised range as in the variation in scaling variables as seen in section 4.3.1. Furthermore, the discount rate was also set to the same discount rate as in the base case study. This variation in average wind speed was achieved by changing the value of the scale parameter of the Weibull distribution, due to its dependence on the average wind speed. The scale parameter is calculated using equation 59.

$$a = \frac{U_{mean}}{\Gamma(1 + \frac{1}{k})} \tag{59}$$

Here, a is the scale parameter, U_{mean} is the average wind speed, Γ is the gamma function and k is the shape parameter. Using equation 59, the scale parameters for wind speeds ranging from 8.5 m/s up to 13 m/s in steps of 0.5 m/s were calculated. The shape parameter was kept constant at 2.3, since offshore variation in the shape parameter is minimal for the Dutch North Sea, as can be seen in figure 32.

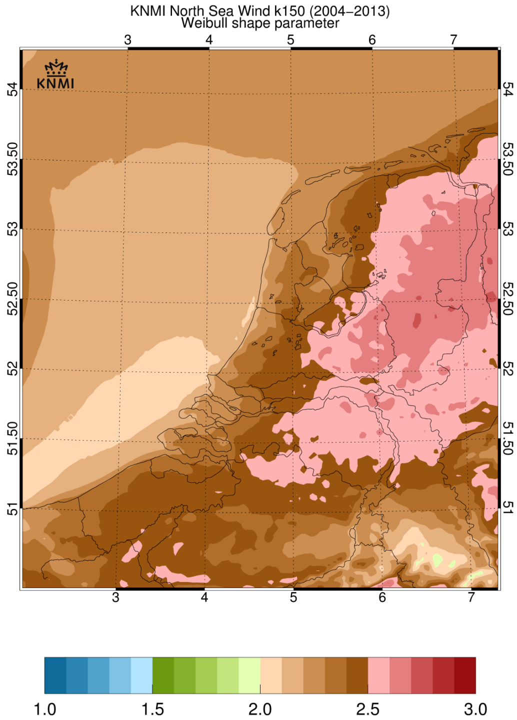

Figure 32: Weibull shape parameters the Netherlands at 150 meters [41]

The summarised results are given in figure 33 and 34. In figure 33, the spread of the optimal power capacity for the different average wind speeds is given. As can be expected, higher average wind speed conditions result in a higher optimal power capacity. It should be noted that the highest average wind speeds have their optimal power capacity cap out at 35 MW. This is because the runs were only performed for a range between 15 and 35 MW.

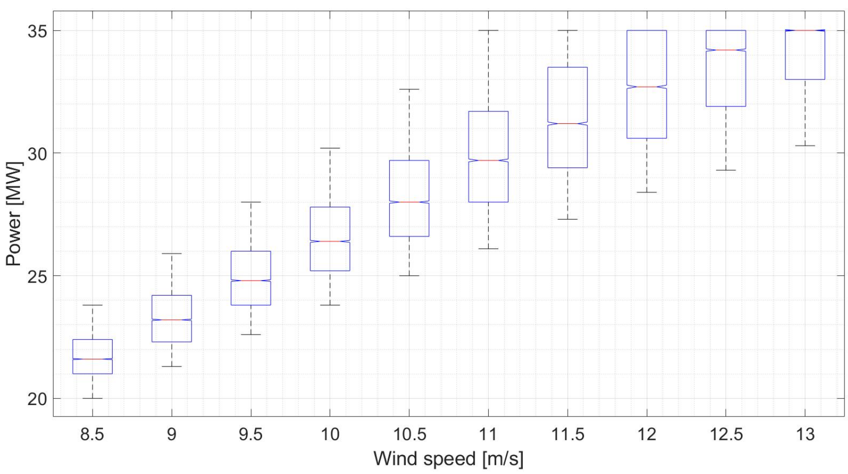

Figure 33: Boxplot of optimal power capacity variation of different average wind speeds

Figure 34 gives the LCoH for the median optimal power capacity for different average wind speeds. The median optimal power capacity was determined in a similar way to that of the discount rate, where for each discount rate, the optimal power was determined, of which the median was taken. For that median, the LCoH is given. The LCoH appears to flatten out after 11 m/s, but this is partially a result of the runs not being performed above 35 MW. Therefore, the LCoH at 35 MW is the minimal achievable. It is also a result of the fact that the amount of extra production flattens out at higher power capacities, due to losses as described above.

As can be seen, a higher wind speed results in a lower LCoH. When a location with an average wind speed of 11.5 m/s but a similar Weibull shape parameter is chosen for the hydrogen turbine wind farm, the green hydrogen has a similar cost to that of grey hydrogen in Europe. A higher average wind speed would even put the green hydrogen at an LCoH lower than that of grey hydrogen.

The main reason for the lower LCoH and higher power capacity at an increased average wind speed is the increase in production. Since a higher average wind speed allows the hydrogen turbines to run at a higher rated wind speed more often, a higher optimal power capacity can be achieved. Furthermore, more often production at rated wind speed means more production. More production lowers the LCoH, as seen in equation 1.

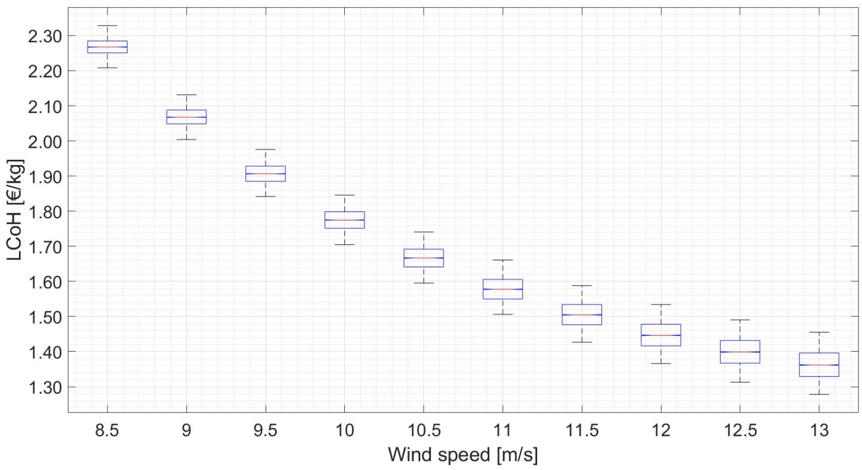

Figure 34: Boxplot of LCoH variation of different average wind speeds at their median optimal rated power

Similar to the discount rate results, the results for the extreme cases of an average wind speed of 8.5 m/s and 13 m/s are given below in figure 35 and 36. The minimal LCoH at 8.5 m/s is achieved between 20 and 25 MW. Within this range, the median LCoH differs around 0.015 €/kg. Furthermore, the LCoH does not achieve a value below 2.25 €/kg. For the 13 m/s scenario, the range lays between 30 and 35 MW and would likely be lower if the results were made up to a higher power capacity level than 35 MW. The difference between the median LCoH at 25 MW and 35 MW is bigger and reaches around 0.05€/kg. This value might be bigger, depending on results in a larger power capacity range.

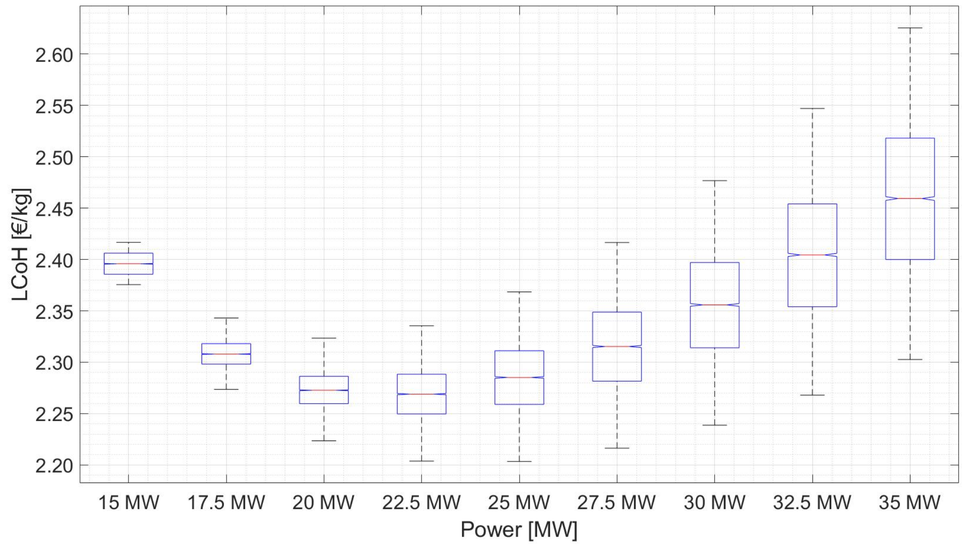

Figure 35: Boxplot of LCoH variation of different power capacities at an average wind speed of 8.5 m/s

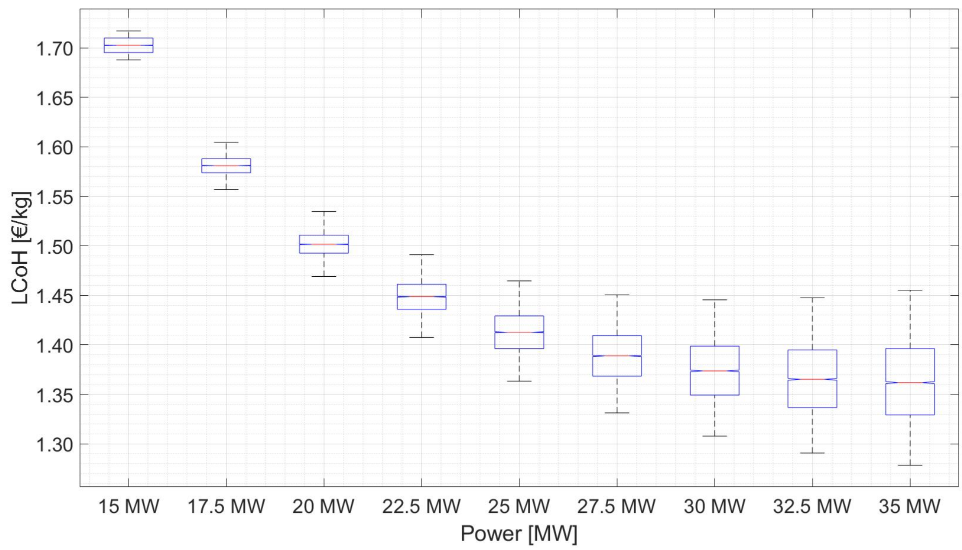

Figure 36: Boxplot of LCoH variation of different power capacities at an average wind speed of 13.0 m/s

5 Conclusion and recommendations

5.1 Conclusions

The goal of providing "advice on a more optimal specific power of hydrogen turbines" has been successful within the boundaries set, such as the constant hub height and maximum rotor speed.

As can be seen from the results of the case study, scaling a hydrogen turbine will lower the LCoH up to a certain point. However, this decrease does not continue on endless and beyond a certain point, a further increase in power capacity and therefore cost increase is not compensated by the increase in production.

The case study results show that when a 15 MW turbine is used as a reference point, the optimal power capacity will lay somewhere between 25 and 31.5 MW, or an increase of power by 67 up to 110%. The results show a higher probability of the optimal power being in the range 25-28 MW rather than above that. Furthermore, the LCoH flattens out around this area, which means that an increase of the power capacity will only have a very minimal effect on the LCoH. Therefore, for a similar sized turbine as that in the case study, an hydrogen turbine would be more optimal with a power capacity of somewhere between 25 and 28 MW instead of 15 MW. This way, an LCoH of around 1.69 €/kg could be achieved. The cost of a 25 MW turbine ranges from €24.9 million up to €26.6 million. A wind farm with 67 of these 25 MW turbines would likely cost between €3,730 million and €3,846 million.

Since the LCoH of grey hydrogen currently is around 1.50 €/kg in Europe, a green hydrogen LCoH of 1.69 €/kg shows a lot of potential for being a competitive options. This is especially true in the scenario where either the grey hydrogen is taxed more due to the emitting of carbon, or green hydrogen is subsidised. It should also be noted that even an unscaled hydrogen turbine appears to be able to achieve an LCoH of around 1.90 €/kg, which suggests that hydrogen turbines have a lot of potential in the (green) hydrogen market.

Based on the results of the case study, it would be advisable to research the potential increase of power capacity for other hydrogen turbines during their development. Furthermore, especially for far offshore locations with higher average wind speeds, hydrogen turbines could result in an LCoH lower than that of grey hydrogen. Hydrogen turbines also are a feasible possibility for far offshore due to the lack of cables. Cables for far offshore locations are problematic due to cost and electricity losses. Modern pipelines do not experience as high losses and could therefore potentially go hundreds of kilometers offshore.

The sensitivity of the model based on the case study is a reason for further research. Especially the effect of the wake factor creates a lot of uncertainty. However, the average resulting optimal specific power is within a constant range, which would suggest that the results are reasonable.

As can be seen through the variation of the discount rate, the economic conditions affect the final result. However, the minimal achieved optimal power capacity is not much lower than the earlier stated likely optimum of 25 - 28 MW. Therefore, only in extremely unfavorable economic conditions, the optimal power capacity will be slightly lower. Furthermore, the LCoH at the optimal power capacity is not likely to be much lower than that of a power capacity between 25 - 28 MW. In a similar way, in extremely favourable economic conditions, the optimal power capacity might be higher than the 25 - 28 MW range, but the LCoH at that higher optimal power is not likely to be much lower.

Within the variation of the wind speed results, the variation does result in a new recommended range. In scenarios of low average wind speeds, the LCoH at the optimal power remains above 2.00 €/kg, making it less feasible as an alternative for grey hydrogen in Europe. It would still be cheaper than the current price of green hydrogen, but not by much. In the scenario of a high average wind speed, the LCoH can drop below the price of grey hydrogen in Europe and achieve an LCoH of up to 1.30 €/kg. Different from the discount rate variation is that the optimal power capacity at either of the extreme wind conditions is in a different range than the previously stated 25 - 28 MW. At power capacities in that range, the LCoH will almost always be at least several cents higher than that of the optimal power capacity. Therefore, different locations can result in different optimal power capacity ranges. However, for near shore locations, the average wind speed will likely result in an optimal level in the previously stated range of 25 - 28 MW. Furthermore, in conditions with much higher average wind speeds, the model is pushed to its limit and will therefore become less reliable.

5.2 Recommendations

Even though the model shows promising results, it has several areas that are more or lesser imperfect. In order to discuss this properly, the model should be split up into a cost and production side. The cost side includes the scaling of the turbine and the farm and all related areas. The production side mainly consists of the production amounts and the loss modelling. As stated in the results chapter, the wake factor has the most effect on the spreading of the results. The wake factor is part of the production side, so that is what will be discussed first.

5.2.1 Production discussion

The production model has two parts that have the most problems. The first is the wake modelling and the second is the fitting of the production curve.

The wake model used is a very simple, linear correlation between the power and the loss. Through a small variation in the amount of production lost due to wake, a large variation in the resulting optimal power and LCoH is found, suggesting a major imperfection. In order to mitigate this imperfection, a proper wake loss model should be included. This would remove most of the uncertainty in the results. Furthermore, the model currently does not make any changes to mitigate the increasing wake losses. Under normal conditions this would also be done and is therefore advised to incorporate in the model as well.

The production curve is currently a fit over nine given data points by HYGRO. Since these data points are only taken at points where the stack size is maximum, the effects of smaller stacks is not taken into account. This could result in a different curve of the production.

5.2.2 Cost discussion

The cost model also has some areas that could be improved upon. It is is advisable to first look at those components that scale the quickest with an increasing power capacity but also are more expensive. This would be the electrolyser, the generator and the blade, since these components affect the cost scaling the most. A cost increase of a cheap component or of a hardly scaling component will not affect the optimal outcome as much.

One of the main components that could be improved upon are the blades. The blades are the third most expensive component and therefore have a big effect on the total turbine cost. The blades currently are not redesigned but have their cost purely based on the expected mass increase. No research has been done on the manufacturing viability, or the non-static effects of a higher power capacity. These areas might raise problems on the scaling of the blades above a certain point. Lastly, no distinguishment has been made between the different materials within the blade. Fully modelling the blade would allow insight in the specific amounts of material and therefore into the exact cost of the blades.

The generator model can also be improved upon. Especially interesting are the possibilities of larger direct drive generators or if different generator solutions are necessary. The generator is also not fully modelled and therefore does not have an exact configuration. A more complete model would result in a more complete overview of the optimal hydrogen turbine.

The power capacities between the 2.5 MW intervals of the electrolyser stack size are not properly incorporate the cost of adding the first kilowatt of an extra stack compared to adding a kilowatt to an almost maximum size stack. This means that the apparent optimal power capacity might be somewhere between these 2.5 MW intervals, but the actual cost of having an electrolyser stack of that size are underestimated.

Other components that could be improved upon by further research are the tower, transition piece and monopile. All three have been scaled through a volume increase based on the forces acting on them. A complete design of all three would result in more insight into, among others, the effects on the natural frequency of the tower and transition piece and a more exact embedment depth.

Within the model, several components were assumed not to scale. However, in all likelihood, these components do scale with an increasing power capacity. The scaling is likely to be minimal and therefore not affect the results much, but it would increase the precision of the resulting turbine designs.

References

[1] HYGRO, Enabling hydrogen from wind, 2020. [Online]. Available: https://hy-gro.net/en.

[2] IEA, Low-carbon hydrogen production, 2010-2030, historical, announced and in the sustainable development scenario, 2030, 2020. [Online]. Available: https://www.iea.org/data-and-statistics/charts/low-carbon-hydrogen-production-2010-2030-historical-announced-and-in-the-sustainable-development-scenario-2030.

[3] Martin Lambert, "Eu hydrogen strategya case for urgent action towards implementation," The Oxford Institute for Energy Studies, Oxford, Tech. Rep., 2020.

[4] IEA, "The future of hydrogen," International Energy Agency, Paris, Tech. Rep., 2019.

[5] TNO, World first: An offshore pilot plant for green hydrogen, 2020. [Online]. Available: https://www.tno.nl/en/focus-areas/energy-transition/roadmaps/towards-co2-neutral-fuels-and-feedstock/hydrogen-for-a-sustainable-energy-supply/world-first-an-offshore-pilot-plant-for-green-hydrogen/.

[6] HYGRO, Hydrogen from wind, 2020. [Online]. Available: https://hy-gro.net/en/waterstof-uit-wind.

[7] Ryan Wiser and Mark Bolinger, "2014 wind technologies market report," U.S. Department of Energy, Tech. Rep., 2015.

[8] IEA, "Definition of the iea 15-megawatt offshore reference wind," International Energy Agency, Denver, Tech. Rep., 2020.

[9] Makanga Koumba Paul, Bekhada Hamane, Mamadou Lamine Doumbia and Ahmed Chériti, "Pitch control of a wind energy conversion system based on permanent magnet synchronous generator (pmsg)," in 2015 Tenth International Conference on Ecological Vehicles and Renewable Energies (EVER), 2015.

[10] PlugPower, Home page plugpower, 2020. [Online]. Available: https://www.plugpower.com/.

[11] Yujing Guo, Gendi Li, Junbo Zhou and Yong Liu, "Comparison between hydrogen production by alkaline water electrolysis and hydrogen production by pem electrolysis," IOP Conference Series: Earth and Environmental Science vol. 371, no. 4, pp. 155–161, 2019.

[12] Howden, Centrifugal, diaphragm, reciprocating, and twin screw compressors, 2020. [Online]. Available: https://www.howden.com/en-gb/products/compressors.

[13] David M. Warsinger, Amelia Servi, Grace B. Connors, Musthafa O. Mavukkandy, Hassan A. Arafat, Karen K. Gleason and John H. Lienhard V, "Reversing membrane wetting in membrane distillation: Comparing dryout to backwashing with pressurized air," Environmental Science: Water Research Technology, vol. 3, pp. 930–939, 2017.

[14] D. E. M. Warsinger, "Thermodynamic design and fouling of membrane distillation systems," Ph.D. dissertation, Massachusetts Institute of Technology, Cambridge, Massachusetts 02139, USA, Jun. 2015.

[15] B. Senthil Rathi and P. Senthil Kumar, "Electrodeionization theory, mechanism and environmental applications. a review," Environmental Chemistry Letters volume, vol. 18, pp. 1209–1227, 2020.

[16] Andrej Grabowski, Guiquing Zhang, Heiner Strathmann and Gerhart Eigenberger, "The production of high purity water by continuous electrodeionization with bipolar membranes: Influence of the anion-exchange membrane permselectivity," Journal of Membrane Science, vol. 281, no. 1–2, pp. 297–306, 2006.

[17] SoluForce, High pressure flexible composite pipe systems, 2020. [Online]. Available: https://www.soluforce.com/product-overview/pipe-types.html.

[18] ——, Soluforce h2t, 2020. [Online]. Available: https://www.soluforce.com/content/dam/pipelife/soluforce/marketing/general/brochures/soluforce-hydrogen-tight-h2t-brochure.pdf.

[19] M.B. Zaaijer and A. Viré, Introduction to wind turbines: physics and technology. 2018.

[20] BVG Associates, "Guide to an offshore wind farm," The Crown Estate, Tech. Rep., 2019.

[21] Ian Webster, U.s. inflation calculator, 2020. [Online]. Available: https://www.in2013dollars.com/.

[22] OFX, Yearly average rates, 2020. [Online]. Available: https://www.ofx.com/en-au/forex-news/historical-exchange-rates/yearly-average-rates/.

[23] NREL, "Manufacturing cost analysis for proton exchange membrane water electrolyzers," National Renewable Energy Laboratory, Denver, Tech. Rep., 2019.

[24] ——, "Wind turbine design cost and scaling model," National Renewable Energy Laboratory, Golden, Tech. Rep., 2006.

[25] ABB, "Abb wind turbine converters, acs880, 800 kw to 8 mw," Tech. Rep., 2020.

[26] Ian Webster, Value of $219.33 from 2002 to 2020, 2020. [Online]. Available: https://www.in2013dollars.com/us/inflation/2002?amount=219.33.

[27] NREL, "Comparative assessment of direct drive high temperature superconducting generators in multi-megawatt class wind turbines," National Renewable Energy Laboratory, Golden, Tech. Rep., 2010.

[28] S. P. Pedro P. Camanho C.G. Dávila and J. Remmers, Mechanical response of composites, ser. Computational Methods in Applied Sciences vol. 10. Springer, 2008, ISBN: 978-1-4020-8583-3.

[29] IEA, "Iea wind task 37 on systems engineering in wind energy wp2.1 reference wind turbines," International Energy Agency, Denver, Tech. Rep., 2019.

[30] NREL, "Windpact turbine rotor design study," National Renewable Energy Laboratory, Golden, Tech. Rep., 2002.

[31] A. Verruijt, "Blum's method laterally loaded piles," TU Delft, Tech. Rep., 1999.

[32] Michiel Zaaijer, "Internal memorandum, document for offshore windfarm design course, support structure design equations," Tech. Rep.

[33] Vincenzo Liso, Giorgio Savoia, Samuel Simon Araya, Giovanni Cinti and Søren Knudsen Kær, "Modelling and experimental analysis of a polymer electrolyte membrane water electrolysis cell at different operating temperatures," Energies, vol. 11, no. 12, p. 3273, 2018.

[34] SPARTA Offshore, "System performance, availability and reliability trend analysis," Tech. Rep., 2019. [Online]. Available: https://www.sparta-offshore.com/SpartaHome#downloads.

[35] GasUnie, Gasunie presenteert resultaten 2019, 2020. [Online]. Available: https://www.gasunie.nl/nieuws/van-gas--naar-energie-infrastructuur-in-een-veranderende-markt.

[36] Siemens Gamesa, Sg 14-222 dd, 2020. [Online]. Available: https://www.siemensgamesa.com/products-and-services/offshore/wind-turbine-sg-14-222-dd.

[37] Directorate-General for Regional and Urban policy, "Guide to cost-benefit analysis of investment projects, economic appraisal tool for cohesion policy 2014-2020," European Commission, Brussels, Tech. Rep., 2015.

[38] FINO1, Location, 2020. [Online]. Available: https://www.fino1.de/en/location.html.

[39] KNMI, F150 wind speed distribution for fino-1 (2004-2013), 2020. [Online]. Available: http://projects.knmi.nl/knw/Plots/WSD/WSD150_FINO1_2004-2013.png.

[40] M.B. Zaaijer, B. Doekemeijer, A. K. Pamososuryo, Nrel fastv8, with matlab gui and simulink integration, 2020. [Online]. Available: https://github.com/TUDelft-DataDrivenControl/FASTTool.

[41] KNMI, Knmi north sea wind a150 (2004 - 2013) weibull scale parameter, 2020. [Online]. Available: http://projects.knmi.nl/knw/Plots/A150_domain_2004-2013.png.

A Matlab scripts

Below, the different Matlab scripts used during this thesis are given. Most of the comments within the scripts were removed for spacial clarity in the report, but are still present in the original script. The scripts FinePitch.m and PerformanceCoefficients.m are based on scripts used in the program FASTTool [40].

A.1 Code.m

MATLAB script 1: Code.m

```
clear all; close all; clc;

%% Error variables
    Infl                = 0.022;
    Inter               = 0.04;
    i_rate              = (1+Inter)/(1+Infl)-1;

    fu                  = 0.8 + (1.2 - 0.8)*rand;
    fu_t                = 0.70 + (1.30-0.70)*rand;
    fu_m                = 0.70 + (1.30-0.70)*rand;
    fu_m2               = 2.98 + (3.005 - 2.98)*rand;

    P_blade             = 12.5 + (16.7-12.5)*rand;
    GeneratorError      = 1 + (1.11-1)*rand;
    Blade_ratio         = 0.6735 + (1-0.6735)*rand;
    WakeFactor          = 4e-6*rand;

   U_mean               = 10.3652;
%% Determine cP, cQ, cT and lambda for blade design
run FinePitch.m

%% Determining new rated wind speeds, cP, cQ and cT for different power values
Power    = 15.1e6:100e3:35e6;

U_r0     = 10.59;
CPmax    = max(CPij);
C1       = 15e6/(CPmax*U_r0^3);
CP       = CPmax;
R        = 120;
omega    = 0.792;
lambda0  = 8.9745;

CQ0      = CPmax/lambda0;
CT0      = CTij(find(abs(Rotor_Lamda-lambda0)<0.0005));
Q0       = C1*R*U_r0^2*CQ0;
T0       = C1*U_r0^2*CT0;

for i = 1:length(Power)

    U_r1(i)  = nthroot(Power(i)/(CP*C1),3);
    lambda1(i)  = round(omega*R/U_r1(i),2);
    Location = find(abs(Rotor_Lamda-lambda1(i))<0.0001);
    CP = CPij(Location);
    CP1(i)  = CP;

    U_r2(i)  = nthroot(Power(i)/(CP*C1),3);
```

```
    lambda2(i) = round(omega*R/U_r2(i),2);
    Location = find(abs(Rotor_Lamda-lambda2(i))<0.0001);
    CP = CPij(Location);
    CP2(i) = CP;

    U_r3(i) = nthroot(Power(i)/(CP*C1),3);
    lambda3(i) = round(omega*R/U_r3(i),2);
    Location = find(abs(Rotor_Lamda-lambda3(i))<0.0001);
    CP = CPij(Location);
    CP3(i) = CP;

    CQ(i) = CP3(i)/lambda3(i);
    CT(i) = CTij(find(abs(Rotor_Lamda-lambda3(i))<0.0001));

    Q(i) = C1*R*U_r3(i)^2*CQ(i);
    T(i) = C1*U_r3(i)^2*CT(i);
end

%% Blades
m_blade0 = 65250;

for i = 1:length(Power)
    TF(i)        = T(i)/T0;
    m_blade(i)   = m_blade0*(TF(i)^Blade_ratio);
end

%% Generator
m_generator0 = 172.8*(Q0/1000)^0.8;

for i = 1:length(Power)
    m_generator(i)                = 172.8*(Q(i)/1000)^0.8;
end

%% Converter system mass
m_converter0 = 0.9618 * 15e3 + 171.5;

for i = 1:length(Power)
    m_converter(i) = 0.9618 * Power(i)/1e3 + 171.5;
end

%% Tower stresses
m_tower0     = 760000;

H            = flipud(Tower.Height);
H            = H-H(21);
H(22:27)     = [];
H0           = flipud(H);

D0           = Tower.Diameter;
t_w0         = Tower.WallThickness/1000;
D0(1:6)      = [];
t_w0(1:6)    = [];

A_bot0       = pi*(D0(1)^2 - (D0(1)-t_w0(1))^2);

tWD          = t_w0(1)/D0(1);
```

```
%Bending stress for bottom
M0           = T0*H(1);
y0           = D0(1)/2;
I0           = (pi/64) * (D0(1)^4-(D0(1)-2*tWD*D0(1))^4);
sigma_bend   = M0*y0/I0;

for i=1:length(Power)
    Vari(i)      = (T(i)*H(1)*64)/(sigma_bend*2*pi*(1-(1-2*tWD)^4));
    D_bot(i)     = Vari(i)^(1/3);
    t_w_bot(i)   = tWD(1)*D_bot(i);
end

%Compression stress for top
m_nacelle_part0 = 196971;
m_hub0          = 190000;
m_bedplate0     = 70329;

for i = 1:length(Power)
    m_hub(i)  = 6.171 * m_blade(i) - 212600;
    m_bedplate(i) = m_bedplate0*(m_hub(i)+m_blade(i)*3+m_generator(i))...
    /(m_hub0+m_blade0*3+m_generator0);
    m_nacelle(i) = m_nacelle_part0 + m_hub(i) + m_bedplate(i);
end

g                   = 9.81;
D_top               = D0(length(D0));
A_top0              = pi*((D_top/2)^2 - ((D_top-2*t_w0(length(t_w0)))/2)^2);
m_top_total0        = 3*m_blade0 + m_generator0 + m_nacelle_part0 + m_hub0 ...
+ m_bedplate0 + m_converter0;

sigma_comp          = g*m_top_total0/A_top0;

for i = 1:length(Power)
    m_top_total(i)  = 3*m_blade(i)+m_generator(i)+m_nacelle(i)+m_converter(i);

    Vari1(i)  = (D_top/2)^2 - g * m_top_total(i)/(pi * sigma_comp);
    t_w_top(i) = D_top/2  - sqrt(Vari1(i));
end

%% Tower mass
for i = 1:length(Power)

        fc_tow(i)        = t_w_top(i)/t_w0(length(t_w0))  * fu - (fu-1);
        fb_tow(i)        = D_bot(i)/D0(1)   * fu - (fu-1);

    for j=1:length(D0)
        zz(j)          = H0(j)/H(length(1));

        t_w1(j,i)     = (t_w0(j) * (zz(j) * fc_tow(i) + (1 - zz(j)) * fb_tow(i)));
        D1(j,i)       =  (D0(j) * (zz(j) + (1 - zz(j)) * fb_tow(i)));

    end

end

```

```
for i = 1:length(D0)
    A0(i) = pi*((D0(i)/2)^2 - ((D0(i)-2*t_w0(i))/2)^2);
end

for i = 2:length(D0)
    V0(i) = A0(i)*(H0(i)-H0(i-1));
end

V0(1)    = [];

for i = 1:length(Power)
    for j = 1:length(D0)
        A1(j,i) = pi*((D1(j,i)/2)^2 - ((D1(j,i)-2*t_w1(j,i))/2)^2);

    end

    for j = 2:length(D0)
        V1(j,i) = A1(j,i)*(H0(j)-H0(j-1));
    end
end

V1(1,:) = [];

for i = 1:length(Power)
    V_to_V1(i) = sum(V1(:,i))/sum(V0);
    m_tower(i) = m_tower0*V_to_V1(i);
 end


%% Transition piece stresses
load TransPiece.mat
m_transipiece0    = 100000;

H_t                = TransPiece.Height;
H0_t               = flipud(H_t);

D0_t               = TransPiece.Diameter;
t_w0_t             = TransPiece.WallThickness/1000;


A_bot0_t           = pi*(D0_t(1)^2 - (D0_t(1)-t_w0_t(1))^2);

for i = 1:length(D0_t)
    tWD_t(i)     = t_w0_t(i)/D0_t(i);
end

%Bending stress for bottom
M0_t             = T0*max(Tower.Height);
y0_t             = D0_t(1)/2;
I0_t             = (pi/64) * (D0_t(1)^4-(D0_t(1)-2*tWD_t(1)*D0_t(1))^4);
sigma_bend_t   = M0_t*y0_t/I0_t;


for i=1:length(Power)
    Vari_t(i)          = (T(i)*(max(Tower.Height)) * 64) / ...
                         (sigma_bend_t * 2 * pi * (1-(1-2*tWD_t(1))^4));
```

```
    D_bot_t(i)          = Vari_t(i)^(1/3);
    t_w_bot_t(i)        = tWD_t(1)*D_bot_t(i);

    fb_t(i)     = (D_bot_t(i)/D0_t(1)) * fu_t - (fu_t-1);
    for j = 1:length(D0_t)
        D_t(j,i)     = D0_t(j)*fb_t(i);
        t_w_t(j,i)   = t_w0_t(j)*fb_t(i);
    end
end

%% Transition piece mass
for i = 1:length(D0_t)
    A0_t(i) = pi*((D0_t(i)/2)^2 - ((D0_t(i)-2*t_w0_t(i))/2)^2);
end

for i = 2:length(D0_t)
    V0_t(i) = A0_t(i-1)*(H0_t(i)-H0_t(i-1));
end
V0_t(1)    = [];

for i = 1:length(Power)
    for j = 1:length(D0_t)
        A_t(j,i)   = pi*((D_t(j,i)/2)^2  - ...
                     ((D_t(j,i) -2*t_w_t(j,i))/2)^2);
    end

    for j = 2:length(D0_t)
        V_t(j,i) = A_t(j-1,i)*(H0_t(j)-H0_t(j-1));
   end
end
V_t(1,:) = [];


for i = 1:length(Power)
    V_to_V0_t(i) = sum(V_t(:,i))/sum(V0_t);
    m_transipiece(i) = m_transipiece0*V_to_V0_t(i);
end


%% Monopile stress
load Monopile.mat
m_monopile0     = 1318000;

H_m             = Monopile.Height;
H0_m            = flipud(H_m)*-1;
H0_m(13)        = 0;

D0_m            = Monopile.Diameter;
t_w0_m          = Monopile.WallThickness/1000;

A_bot0_m        = pi*(D0_m(1)^2 - (D0_m(1)-t_w0_m(1))^2);

for i = 1:length(D0_m)
    tWD_m(i)     = t_w0_m(i)/D0_m(i);
end

```

```
%Bending stress for bottom
M0_m            = T0*(max(Tower.Height) - H_m(1));
y0_m            = D0_m(1)/2;
I0_m            = (pi/64) * (D0_m(1)^4-(D0_m(1)-2*tWD_m(1)*D0_m(1))^4);
sigma_bend_m    = M0_m*y0_m/I0_m;

for i=1:length(Power)
    Vari_m(i)           = (T(i)*(max(Tower.Height) - H_m(1)) * 64)/...
                          (sigma_bend_m * 2 * pi * (1-(1-2*tWD_m(1))^4));
    D_bot_m(i)          = Vari_m(i)^(1/3);
    t_w_bot_m(i)        = tWD_m(1)*D_bot_m(i);

    fb_m(i)     = (D_bot_m(i)/D0_m(1)) * fu_m - (fu_m-1);

    for j = 1:length(D0_m)
        D_m(j,i)  = D0_m(j)*fb_m(i);
        t_w_m(j,i)  = t_w0_m(j)*fb_m(i);
    end
end

%% Monopile volume
for i = 1:length(D0_m)
    A0_m(i)  = pi*((D0_m(i)/2)^2 - ((D0_m(i)-2*t_w0_m(i))/2)^2);
end

for i = 1:length(D0_m)
    V0_m_top(i)  = A0_m(i)*(H0_m(i)-H0_m(i+1));
end

for i = 1:length(Power)
    for j = 1:length(D0_m)
        A_m(j,i)   = pi*((D_m(j,i)/2)^2 - ...
                         ((D_m(j,i) - 2 * t_w_m(j,i))/2)^2);
    end

    for j = 1:length(D0_m)
        V_m_top(j,i)  = A_m(j,i)*(H0_m(j)-H0_m(j+1));

    end
end

%% Sub sea-bed Monopile
H_sub0              = 45;
M_over0             = T0*(max(Tower.Height));
V0_m_sub            = A0_m(1)*H_sub0;
F_sub0              = T0;

for i = 1:length(Power)
    F_sub(i)              = T(i);
    M_over(i)             = T(i)*(max(Tower.Height));
end

H_sub20             = H_sub0/1.3;

Constant1 = 6*M_over0 /((H_sub20^3)* D0_m(1));
Constant2 = 6*F_sub0 / ((H_sub20^2)* D0_m(1));
```

```
for i = 1:length(Power)
    H_sub(i)    = 1.3*nthroot((6*M_over(i)/(Constant1*D_m(1,i))),fu_m2);
    V_m_sub(i)  = A_m(1,i) * H_sub(i);
end

%% New Mass monopile
V0_m                = sum(V0_m_top) + V0_m_sub;


for i = 1:length(Power)
    V_m(i)          = sum(V_m_top(:,i)) + V_m_sub(i);

    V_to_V0_m(i)    = V_m(i)/V0_m;
    m_monopile(i)   = m_monopile0*V_to_V0_m(i);
end



%% Cost of single turbine
C_elyser0       = 15e6*0.3;
C_tower0        = m_tower0*1.36;
C_blades0       = m_blade0*3*P_blade;
C_generator0    = 15e6*0.25;
C_hub0          = m_hub0*3.45;
C_yaw0          = (276e3/193)*240;
C_pitch0        = (115e3/193)*240;
C_controlsys0   = 287500;
C_bearings0     = (230e3/193)*240;
C_bedplate0     = m_bedplate0 * 5.23;
C_converter0    = 34.43*15e3;
C_shaft0        = (230e3/193)*240;
C_misc0         = 611500;
C_monopile0     = m_monopile0*0.8625;
C_transipiece0  = m_transipiece0*2.3;
C_pump0         = 100e3 + 15e6*0.048;


C_total0        = C_tower0 + C_elyser0 + C_blades0 + C_generator0 + ...
                    C_hub0 + C_yaw0 + C_pitch0 + C_controlsys0 + ...
                    C_bearings0 + C_converter0 + C_bedplate0 + ...
                    C_shaft0 + C_misc0 + C_monopile0 + ...
                    C_transipiece0 + C_pump0;

for i = 1:length(Power)
    C_elyser(i)         = Power(i) * 0.3;
    C_tower(i)          = m_tower(i) * 1.36;
    C_blades(i)         = m_blade(i) * 3 * P_blade;
    C_generator(i)      = ((Power(i)/15e6)^GeneratorError)*15e6 * 0.25 ;
    C_hub(i)            = m_hub(i) * 3.45;
    C_yaw(i)            = C_yaw0;
    C_pitch(i)          = C_pitch0;
    C_controlsys(i)     = C_controlsys0;
    C_bearings(i)       = C_bearings0;
    C_bedplate(i)       = m_bedplate(i) * 5.23;
    C_converter(i)      = 34.43 * Power(i)/1000;
```

```
    C_shaft(i)           = C_shaft0;
    C_misc(i)            = C_misc0;
    C_monopile(i)        = m_monopile(i)*0.8625;
    C_transipiece(i)     = m_transipiece(i)*2.3;
    C_pump(i)            = 100e3 + Power(i)*0.048;

% Total
    C_total(i)           = C_tower(i) + C_elyser(i) + C_blades(i) + ...
                             C_generator(i) + C_hub(i) + C_yaw(i) + ...
                             C_pitch(i) + C_controlsys(i) + ...
                             C_bearings(i) + C_converter(i) + ...
                             C_bedplate(i) + C_shaft(i) + C_misc(i) + ...
                             C_monopile(i) + C_transipiece(i) + C_pump(i);

end

%% Production
LT                           = 20;
X                            = 67;
Losses                       = (0.95*.997);


[FINO0,FINO,Wake0,Wake]      = Production(LT,WakeFactor,U_mean,X,...
                                         i_rate,Losses);


%% Cost of 67 turbine wind farm


C_instal0                = 1725000*X;


C_operations0(2:21,1)    = 28750000;
C_operations0            = pvvar(C_operations0,i_rate);
C_maintenance0(2:21,1)   = 57500000;
C_maintenance0           = pvvar(C_maintenance0,i_rate);

C_decom0(21,1)           = 2875000*X;
C_decom0                 = pvvar(C_decom0,i_rate);


Distance                 = 60000;
C_pipe0                  = 1.25*Distance*X*15;
C_pipeinstal0            = 4083.333*Distance;

C_turbtotal0             = C_total0*X;

C_farm0                  = C_turbtotal0 + C_instal0 + C_decom0 + ...
                             C_operations0 + C_maintenance0 + ...
                             C_pipe0 + C_pipeinstal0;

for i = 1:length(Power)
    C_instal(i)          = C_instal0;
    C_operations(i)      = C_operations0;
    C_maintenance(i)     = C_maintenance0;
    C_decom(i)           = C_decom0;
```

```
    C_pipeinstal(i)      = C_pipeinstal0;
    C_pipe(i)            = 1.25*Distance*X*Power(i)/1e6;
    C_turbtotal(i)       = C_total(i)*X;
    C_farm(i)            = C_turbtotal(i) + C_instal(i) + C_decom(i) + ...
                             C_operations(i) + C_maintenance(i) + ...
                             C_pipe(i) + C_pipeinstal(i);
end
%%
Prod_cost_FINO0          = C_farm0/FINO0;
Prod_cost_FINO           = C_farm./FINO;
```

A.2 Production.m

MATLAB script 2: Production.m

```
function [FINO0,FINO,Wake0,Wake] = ...
    Production(LT,WakeFactor,U_mean,X,i_rate,Losses)
%% Load power curves
load PowerCurves.mat

U_mean = U_mean;

t            = 8760;
Power        = [15,17.5,20,22.5,25,27.5,30,32.5,35]*1e6;
PowerGoal    = 15e6:0.1e6:35e6;
Power2       = 15.1e3:0.1e3:35e3;
Power0       = 15e3;


Wake0        = 0.9;
for i = 1:length(Power2)
    Wake(i)  = Wake0 - (2e-6 + WakeFactor) * (Power2(i) - Power0);
end

%% FINO-1
k_FINO = 2.3;
A_FINO = 11.7;  % can also be U_mean/(gamma(1+1/k_FINO));
x_FINO = 0:0.5:30;
y_FINO = wblpdf(x_FINO,A_FINO,k_FINO);

t_FINO = t*y_FINO/2;

for i = 1:61
    Prod15MW_FINO(i)     = t_FINO(i)*PowerCurves15MW(i,3);
    Prod175MW_FINO(i)    = t_FINO(i)*PowerCurves175MW(i,3);
    Prod20MW_FINO(i)     = t_FINO(i)*PowerCurves20MW(i,3);
    Prod225MW_FINO(i)    = t_FINO(i)*PowerCurves225MW(i,3);
    Prod25MW_FINO(i)     = t_FINO(i)*PowerCurves25MW(i,3);
    Prod275MW_FINO(i)    = t_FINO(i)*PowerCurves275MW(i,3);
    Prod30MW_FINO(i)     = t_FINO(i)*PowerCurves30MW(i,3);
    Prod325MW_FINO(i)    = t_FINO(i)*PowerCurves325MW(i,3);
    Prod35MW_FINO(i)     = t_FINO(i)*PowerCurves35MW(i,3);
end

Prod15MW_FINO    = sum(Prod15MW_FINO);
```

```
Prod175MW_FINO  = sum(Prod175MW_FINO);
Prod20MW_FINO   = sum(Prod20MW_FINO);
Prod225MW_FINO  = sum(Prod225MW_FINO);
Prod25MW_FINO   = sum(Prod25MW_FINO);
Prod275MW_FINO  = sum(Prod275MW_FINO);
Prod30MW_FINO   = sum(Prod30MW_FINO);
Prod325MW_FINO  = sum(Prod325MW_FINO);
Prod35MW_FINO   = sum(Prod35MW_FINO);

%% Lifetime FINO-1
Prod15MW_FINO_LT    = 0;
Prod175MW_FINO_LT   = 0;
Prod20MW_FINO_LT    = 0;
Prod225MW_FINO_LT   = 0;
Prod25MW_FINO_LT    = 0;
Prod275MW_FINO_LT   = 0;
Prod30MW_FINO_LT    = 0;
Prod325MW_FINO_LT   = 0;
Prod35MW_FINO_LT    = 0;

for i = 1:LT
    Prod15MW_FINO_LT(i)     = Prod15MW_FINO*0.995^(i-1);
    Prod175MW_FINO_LT(i)    = Prod175MW_FINO*0.995^(i-1);
    Prod20MW_FINO_LT(i)     = Prod20MW_FINO*0.995^(i-1);
    Prod225MW_FINO_LT(i)    = Prod225MW_FINO*0.995^(i-1);
    Prod25MW_FINO_LT(i)     = Prod25MW_FINO*0.995^(i-1);
    Prod275MW_FINO_LT(i)    = Prod275MW_FINO*0.995^(i-1);
    Prod30MW_FINO_LT(i)     = Prod30MW_FINO*0.995^(i-1);
    Prod325MW_FINO_LT(i)    = Prod325MW_FINO*0.995^(i-1);
    Prod35MW_FINO_LT(i)     = Prod35MW_FINO*0.995^(i-1);
end

for i = 1:LT
    FINO1(i,:) = [Prod15MW_FINO_LT(i), Prod175MW_FINO_LT(i), ...
                  Prod20MW_FINO_LT(i), Prod225MW_FINO_LT(i), ...
                  Prod25MW_FINO_LT(i), Prod275MW_FINO_LT(i), ...
                  Prod30MW_FINO_LT(i), Prod325MW_FINO_LT(i), ...
                  Prod35MW_FINO_LT(i)];
end

Prod_FINO1                = FINO1*X*Losses;
Prod_FINO1              = pvvar(Prod_FINO1,i_rate);

%%
f1 = fit(Power',Prod_FINO1','power2');

FINO(1,:) = f1(PowerGoal);

FINO0 = FINO(1);
FINO(:,1) = [];

FINO0 = FINO0*Wake0;

for i = 1:200
    FINO(:,i) = FINO(:,i)*Wake(i);
end
```

```
end
```

A.3 FinePitch.m

MATLAB script 3: FinePitch.m

```
load IEA15MW

Pitchi = [];
Pitchi = [Pitchi, Control.Pitch.Fine];


if ~isempty(Pitchi)

    disp('Calculating␣rotor␣performance...')

    TSRj = 0:0.0001:20;
    CPij = zeros(length(Pitchi), length(TSRj));
    CTij = zeros(length(Pitchi), length(TSRj));
    CQij = zeros(length(Pitchi), length(TSRj));
    lgd_label = cell(1, length(Pitchi));

    for i = 1:length(Pitchi)
        disp(['Pitch␣angle␣=␣', num2str(Pitchi(i))])
        lgd_label{i} = [num2str(Pitchi(i), '%.4f'), '␣deg'];
        for j = 10001:length(TSRj)


                disp(['TSR␣=␣', num2str(TSRj(j))])


            [CTij(i,j), CQij(i,j)] = PerformanceCoefficients(Blade, ...
                                        Airfoil, Pitchi(i), TSRj(j));
            CPij(i,j) = CQij(i,j)*TSRj(j);

            if CPij(i,j) < 0 && TSRj(j) > 1
                CPij(i,j) = 0;
                CQij(i,j) = 0;
                break
            end
        end
    end

    % Plot
    disp('Drawing␣plots...')
    Fig = figure();
    set(Fig, 'Name', 'Power␣coefficient␣curve')
    plot(TSRj,CPij(1,:))
    xlim([0 max(TSRj)])
    ylim([0 ceil(20*max(max(CPij)))/20+0.05])
    set(gca, ...
        'XMinorTick', 'on', ...
        'YMinorTick', 'on', ...
        'Box', 'on', ...
```

```
        'Layer', 'top', ...
        'Fontsize', 20);
    xlabel('Tip␣speed␣ratio␣[-]')
    ylabel('Power␣coefficient␣[-]')
    hold on
    for i = 2:length(Pitchi)
        plot(TSRj,CPij(i,:))
    end
    hold off
    grid on

    % Send data to Matlab workspace
    assignin('base', 'Rotor_Pitch', Pitchi(:));
    assignin('base', 'Rotor_Lamda', TSRj(:));
    assignin('base', 'Rotor_cP', CPij);
    assignin('base', 'Rotor_cT', CTij);
    assignin('base', 'Rotor_cQ', CQij);
end
```

A.4 PerformanceCoefficients.m

MATLAB script 4: PerformanceCoefficients.m

```

function [CT, CQ] = PerformanceCoefficients(Blade, Airfoil, pitch, lambda)

r = Blade.Radius/Blade.Radius(end);

CQ = 0;
CT = 0;

for k = 1:(length(Blade.Radius)-1)
    % Initialise search for induction factor (where blade element and
    % momentum theory give equal thrust coefficient)
    a1 = -0.4;
    a2 = 0.80; % 0.99; Induction factor can go up to 1 with this model,
    % but a2 = 0.99 gives convergence problems
    [~, CTBE1, CTMT1] = BEM(a1, k, Blade, Airfoil, pitch, lambda);
    [~, CTBE2, CTMT2] = BEM(a2, k, Blade, Airfoil, pitch, lambda);
    Diff1 = CTBE1 - CTMT1;
    Diff2 = CTBE2 - CTMT2;
    success = false;

    for iter = 1:100
        a = a1 + abs(Diff1/(Diff1-Diff2))*(a2-a1);
        [dCQ, CTBE, CTMT] = BEM(a, k, Blade, Airfoil, pitch, lambda);
        Diff = CTBE - CTMT;
        if abs(Diff) < 0.005
            success = true;
            break
        end
        if Diff*Diff1 > 0 % Difference of equal sign
           a1 = a;
           Diff1 = Diff;
        else
```

```
            a2 = a;
            Diff2 = Diff;
        end
    end
    if ~success
        warning('Tolerance␣not␣met␣during␣iteration␣...
␣␣␣␣␣␣␣␣of␣axial␣induction␣factor')
    end

    % Add coefficients
    % (2*r is a weighing factor for increasing annulus with r)
    CQ = CQ+(r(k+1)-r(k))*dCQ*2*r(k);
    dCT = (r(k+1)-r(k))*(CTBE+CTMT)/2;
    CT = CT+dCT*2*r(k);
end

function [dCQ, CTBE, CTMT] = BEM(a, k, Blade, Airfoil, pitch, lambda)

r = Blade.Radius(k)/Blade.Radius(end);
lambdar = lambda * r;
sigmar = Blade.Number*Blade.Chord(k)/(2*pi*Blade.Radius(k));

% Iteration of tangential induction factor
a_old = 0;
success = false;
for iter = 1:100
    % Inflow angleclose all force
    phi = atan((1-a)/((1+a_old)*lambdar));

    % Tip loss correction
    F = 2/pi * acos(exp(-Blade.Number/2*(1-r)/(r*sin(abs(phi)))));

    % Angle of attack
    alpha = phi*180/pi - pitch - Blade.Twist(k);

    % Aerodynamic force coefficients
    [~,ia] = unique(Airfoil.Alpha{Blade.IFoil(Blade.NFoil(k))});
    Cl = interp1(Airfoil.Alpha{Blade.IFoil(Blade.NFoil(k))}(ia),...
            Airfoil.Cl{Blade.IFoil(Blade.NFoil(k))}(ia), alpha);
    Cd = interp1(Airfoil.Alpha{Blade.IFoil(Blade.NFoil(k))}(ia),...
            Airfoil.Cd{Blade.IFoil(Blade.NFoil(k))}(ia), alpha);

    % Tangential induction factor
    a_ = 1/(4*F*cos(phi)/(sigmar*Cl)-1);

    % Convergence check
    if abs(a_ - a_old) < 0.002
        success = true;
        break
    end
    a_old = a_;
end
if ~success
    warning('Tolerance␣not␣met␣during␣iteration␣of␣tangential␣...
␣␣␣␣␣␣␣␣␣␣␣␣induction␣factor')
end
```

```
% Thrust coefficient per rotor annulus (blade element theory)
CTBE = sigmar*(1-a)^2*(Cl*cos(phi)+Cd*sin(phi))/(sin(phi)^2);

% Thrust coefficient per rotor annulus (momentum theory)
if a <= 0.4
    CTMT = 4*a*(1-a)*F;
else
    CTMT = 8/9 + (4*F-40/9)*a + (50/9-4*F)*a^2; % High induction
                                %(heavy loading) according to Buhl
end

% Torque coefficient per rotor annulus
% Derived directly from tangential force
dCQ = sigmar*r*(Cl*sin(phi)-Cd*cos(phi))*(1-a)^2/(sin(phi)^2);
%{
% Derived from contribution to torque according to Hansen
% (gives almost equal results)
dCQ = lambda*(1-a)*(1+a_)*r^2*sigmar*(Cl*sin(phi)-Cd*cos(phi))/...
        (sin(phi)*cos(phi));
%}
```